

# Finite Element solution of the fiber/matrix interface crack problem: convergence properties and mode mixity of the Virtual Crack Closure Technique

Luca Di Stasio<sup>a,b</sup>, Zoubir Ayadi<sup>b</sup>

<sup>a</sup>*Luleå University of Technology, University Campus, SE-97187 Luleå, Sweden*

<sup>b</sup>*Université de Lorraine, EEIGM, IJL, 6 Rue Bastien Lepage, F-54010 Nancy, France*

---

## Abstract

The bi-material interface arc crack has been the focus of interest in the composite community, where it is usually referred to as the fiber-matrix interface crack. In this work, we investigate the convergence properties of the Virtual Crack Closure Technique (VCCT) when applied to the evaluation of the Mode I, Mode II and total Energy Release Rate of the fiber-matrix interface crack in the context of the Finite Element Method (FEM). We first propose a synthetic vectorial formulation of the VCCT. Thanks to this formulation, we study the convergence properties of the method, both analytically and numerically. It is found that Mode I and Mode II Energy Release Rate (ERR) possess a logarithmic dependency with respect to the size of the elements in the crack tip neighborhood, while the total ERR is independent of element size.

*Keywords:* Fiber/matrix interface crack, Bi-material interface arc crack, Linear Elastic Fracture Mechanics (LEFM), Virtual Crack Closure Technique (VCCT), Mode separation, Convergence

---

## 1. Introduction

Bi-material interfaces represent the basic load transfer mechanism at the heart of Fiber Reinforced Polymer Composite (FRPC) materials. They are present at the macroscale, in the form of adhesive joints; at the mesoscale, as  
5 interfaces between layers with different orientations; at the microscale, as fiber-

matrix interfaces. Bi-material interfaces have for long attracted the attention of researchers in Fracture Mechanics [1, 2], due to their hidden complexity.

The problem was first addressed in the 1950's by Williams [3], who derived through a linear elastic asymptotic analysis the stress distribution around an  
 10 *open* crack (i.e. with crack faces nowhere in contact for any size of the crack) between two infinite half-planes of dissimilar materials. He found the existence of a strong oscillatory behavior in the stress singularity at the crack tip of the form

$$r^{-\frac{1}{2}} \sin(\varepsilon \log r) \quad \text{with} \quad \varepsilon = \frac{1}{2\pi} \log \left( \frac{1-\beta}{1+\beta} \right), \quad (1)$$

in both Mode I and Mode II. In Eq. 1,  $\beta$  is one of the two parameters  
 15 introduced by Dundurs [4] to characterize bi-material interfaces:

$$\beta = \frac{\mu_2 (\kappa_1 - 1) - \mu_1 (\kappa_2 - 1)}{\mu_2 (\kappa_1 + 1) + \mu_1 (\kappa_2 + 1)} \quad (2)$$

where  $\kappa = 3 - 4\nu$  in plane strain and  $\kappa = \frac{3-4\nu}{1+\nu}$  in plane stress,  $\mu$  is the shear modulus,  $\nu$  Poisson's coefficient, and indexes 1, 2 refer to the two bulk materials joined at the interface. Defining  $a$  as the length of the crack, it was found that the size of the oscillatory region is in the order of  $10^{-6}a$  [5]. Given  
 20 the oscillatory behaviour of the crack tip singularity of Eq. 1, the definition of Stress Intensity Factor (SIF)  $\lim_{r \rightarrow 0} \sqrt{2\pi r} \sigma$  diverges and ceases to be valid [1]. It implies that the Mode mixity problem at the crack tip is ill-posed.

It was furthermore observed, always in the context of Linear Elastic Fracture Mechanics (LEFM), that an interpenetration zone exists close to the crack  
 25 tip [6, 7] with a length in the order of  $10^{-4}a$  [6]. Following conclusions firstly proposed in [7], the presence of a *contact zone* in the crack tip neighborhood, of a length to be determined from the solution of the elastic problem, was introduced in [8] and shown to provide a physically consistent solution to the straight bi-material interface crack problem.

30 The curved bi-material interface crack, more often referred to as the fiber-matrix interface crack (or debond) due to its relevance in FRPCs, was first treated by

England [9] and by Perlman and Sih [10], who provided the analytical solution of stress and displacement fields for a circular inclusion with respectively a single debond and an arbitrary number of debonds. Building on their work,  
35 Toya [11] particularized the solution and provided the expression of the Energy Release Rate (ERR) at the crack tip. The same problems exposed previously for the *open* straight bi-material crack were shown to exist also for the *open* fiber-matrix interface crack: the presence of strong oscillations in the crack tip singularity and onset of crack face interpenetration at a critical flaw size.<sup>1</sup>

40 In order to treat cases more complex than the single partially debonded fiber in an infinite matrix of [9, 10, 11], numerical studies followed. In the 1990's, Paris and collaborators [12] developed a Boundary Element Method (BEM) with the use of discontinuous singular elements at the crack tip and the Virtual Crack Closure Integral (VCCI) [13] for the evaluation of the Energy Release Rate  
45 (ERR). They validated their results [12] with respect to Toya's analytical solution [11] and analyzed the effect of BEM interface discretization on the stress field in the neighborhood of the crack tip [14]. Following Comninou's work on the straight crack [8], they furthermore recognized the importance of contact to retrieve a physical solution avoiding interpenetration [12] and studied the effect  
50 of the contact zone on debond ERR [15]. Their algorithm was then applied to investigate the fiber-matrix interface crack under different geometrical configurations and mechanical loadings [16, 17, 18, 19, 20, 21, 22].

Recently the Finite Element Method (FEM) was also applied to the solution of the fiber-matrix interface crack problem [23, 24, 25], in conjunction with the  
55 Virtual Crack Closure Technique (VCCT) [26, 27] for the evaluation of the ERR at the crack tip. In [23], the authors validated their model with respect to the BEM results of [12], but no analysis of the effect of the discretization in the crack tip neighborhood comparable to [14] was proposed. [Thanks to the inter-](#)

---

<sup>1</sup>For the fiber-matrix interface crack, flaw size is measured in terms of the angle  $\Delta\theta$  subtended by half of the arc-crack, i.e.  $\alpha = 2\Delta\theta R_f$  where  $R_f$  is the inclusion (fiber) radius and  $\Delta\theta$  is expressed in radians  $\alpha = 2\Delta\theta$ .

est in evaluating the ERR of interlaminar delamination, different studies exist  
60 in the literature on the effect of mesh discretization on Mode I and Mode II  
ERR of the straight bi-material interface crack when evaluated with the VCCT  
in the context of the FEM (see for example [28] for a review). An early result  
on the problem is available in [29]. Here the authors evaluated with the Virtual  
Crack Closure Technique Mode I and Mode II Energy Release Rate of both a  
65 central crack and an edge crack at the interface between two 2D plates of differ-  
ent isotropic materials subjected to tensile loading. They showed analytically  
that the total ERR  $G$  is well defined while Mode I and Mode II ERR, respec-  
tively  $G_I$  and  $G_{II}$ , do not converge. They confirmed their analytical derivations  
numerically by solving the two problems with the Finite Element Method and  
70 evaluating the ERR with the VCCT. Referring to the crack length as  $a$  and  
to the length of an element at the crack tip as  $\Delta a$ , they found that the total  
ERR was independent of normalized element size  $\Delta a/a$  while  $G_I$  and  $G_{II}$  were  
dependent on assumed crack extension, i.e. element size at the crack tip. In  
particular, they showed a decreasing  $G_I$  and an increasing  $G_{II}$  with decreasing  
75 element size for both crack configurations. The same analysis was conducted,  
and analogous results obtained, in [30] for a central crack under either far-field  
tensile or shear loading between two orthotropic materials in 2D and in [31] for a  
central crack subjected to far-field tension between two orthotropic solids in 3D.  
The convergence of VCCT-based mode decomposition was analyzed in [32] for  
80 edge delaminations in laminated composites subjected to tensile loading copla-  
nar and normal to crack propagation direction in a quasi-3D setting. Again, it  
was observed that the total ERR was independent of mesh size while Mode I  
and Mode II ERR showed dependency and no convergence could be established.  
In this configuration however, it was found that  $G_I$  increases and  $G_{II}$  decreases  
85 with decreasing element size. The application of the VCCT to the problem of  
composite skin-stiffener debonding was considered in [33] in conjunction with  
2D plate elements, where the authors studied the effect of different combinations  
of adherends' layup, thickness and fiber orientation at the interface on Mode  
decomposition. Only in the case of skin and stiffener with the same layup, same

90 thickness and identical fiber orientation at the interface, Mode I and Mode II  
 were found to be independent of mesh size. In all other cases,  $G_I$  and  $G_{II}$  were  
 dependent on assumed crack extension and showed a trend similar to the one  
 in [32]. The absence of a converging Mode-decomposed solution with the VCCT  
 has motivated proposals for alternative solution. In [34], the authors analyze  
 95 several proposals of mode-mixity parameters and suggest a correction to the  
 VCCT-based mode-mixity ratio by assuming a reference characteristic length.  
 The authors themselves however admit that this characteristic length has no  
 physical interpretation. In [35], the problem of Mode-decomposition is solved  
 through the development of analytical relations based on Euler and Timoshenko  
 100 beam models. It is however well suited only for those configurations that can  
 be split into beam elements, such as the Double Cantilever Beam (DCB) speci-  
 men. ~~Thanks to the interest in evaluating the ERR of interlaminar delamination,~~  
~~different studies exist in the literature on the effect of mesh discretization on~~  
~~Mode I and Mode II ERR of the bi-material interface crack when evaluated with~~  
 105 ~~the VCCT in the context of the FEM.~~  
~~However,~~ No comparable analysis can be found in the literature on Mode sepa-  
 ration and convergence analysis of the VCCT when applied to the fiber-matrix  
 interface crack (circular bi-material interface crack) problem in the context of  
 a linear elastic FEM solution. In the present article, we first present the FEM  
 110 formulation of the problem, together with the main geometrical characteristics,  
 material properties, boundary conditions and loading. We then propose a vec-  
 torial formulation of the VCCT and express Mode I and Mode II ERR in terms  
 of FEM natural variables. ~~Differently from the usual approach found in the~~  
~~literature, we do not express  $G_I$  and  $G_{II}$  as functions of stress and displace-~~  
 115 ~~ment fields using the results from complex analysis. We instead focus on the~~  
~~mathematical structure of the 1-step VCCT in the context of the Finite Ele-~~  
~~ment Method and write the crack tip forces as a linear combination of the crack~~  
~~faces displacements at the crack tip (plus a term representing the influence of~~  
~~the rest of the model). The ERR is consequently a quadratic function of the~~  
 120 ~~crack faces displacements. Given that, if the FEM solution is converging, stress~~

and displacement fields are characterized by the oscillating singularity of Equation 1, it is possible to evaluate the behavior of the VCCT-calculated Energy Release Rate in the limit of crack tip element size going to zero. We are thus able to derive analytically a functional form of the dependency of the ERR on crack tip element size. Finally, the functional form thus derived is compared to the numerical results obtained with the Finite Element Method. ~~With this tool, we derive an analytical estimate of the ERR convergence and compare it with numerical results.~~

## 2. FEM formulation of the fiber-matrix interface crack problem

In order to investigate the fiber-matrix interface crack problem, a 2-dimensional model of a single fiber inserted in a rectangular matrix element is considered (see Figure 1). Total element length and height are respectively  $2L$  and  $L$ , where  $L$  is determined by the fiber radius  $R_f$  and the fiber volume fraction  $V_f$  by

$$L = \frac{R_f}{2} \sqrt{\frac{\pi}{V_f}}. \quad (3)$$

The fiber radius  $R_f$  is assumed to be equal to  $1 \mu m$ . This choice is not dictated by physical considerations but for simplicity. It is thus useful to remark that, in a linear elastic solution as the one considered in the present work, the ERR is proportional to the geometrical dimensions of the model and, consequently, recalculation of the ERR for fibers of any size requires a simple multiplication.

As shown in Fig. 1, the debond is placed symmetrically with respect to the  $x$  axis and its size is characterized by the angle  $\Delta\theta$  (which makes the full debond size equal to  $2\Delta\theta$  and the full crack length equal to  $R_f 2\Delta\theta$ ). A region  $\Delta\Phi$  of unknown size appears at the crack tip for large debond sizes (at least  $\geq 60^\circ - 80^\circ$ ), in which the crack faces are in contact with each other and free to slide. Frictionless contact is thus considered between the two crack faces to allow free sliding and avoid interpenetration. Symmetry with respect to the  $x$  axis is applied on the lower boundary while the upper surface is left free. Kinematic

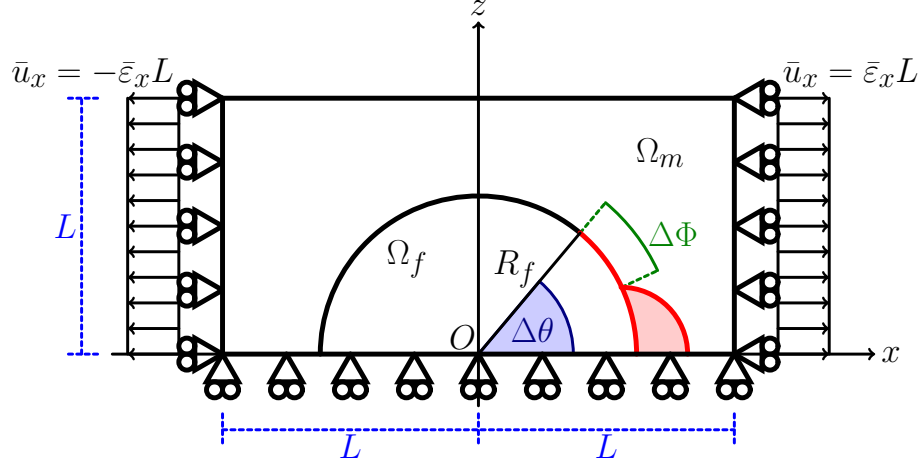


Figure 1: Schematic of the model with its main parameters.

coupling on the  $x$ -displacement is applied along the left and right sides of the model in the form of a constant  $x$ -displacement  $\pm\bar{\varepsilon}_x L$ , which corresponds to  
150 transverse strain  $\bar{\varepsilon}_x$  equal to 1% in the results here presented.

Table 1: Summary of the mechanical properties of fiber and matrix.  $E$  stands for Young's modulus,  $\mu$  for shear modulus and  $\nu$  for Poisson's ratio.

Material	$E$ [GPa]	$\mu$ [GPa]	$\nu$ [-]
Glass fiber	70.0	29.2	0.2
Epoxy	3.5	1.25	0.4

The model problem is solved with the Finite Element Method (FEM) within the Abaqus environment, a commercial FEM software [36]. The model is meshed with second order, 2D, plane strain triangular (CPE6) and rectangular (CPE8) elements. A regular mesh of rectangular elements with almost unitary aspect  
155 ratio is used at the crack tip. The angular size  $\delta$  of an element in the crack tip neighborhood represents the main parameter of the numerical analysis. The crack faces are modeled as element-based surfaces and a small-sliding contact pair interaction with no friction is imposed between them. The Mode I, Mode II and total Energy Release Rates (ERRs) (respectively referred to as  $G_I$ ,  $G_{II}$  and

160  $G_{TOT}$ ) are evaluated using the VCCT [27], implemented in a in-house Python routine. A glass fiber-epoxy system is considered in the present work, and it is assumed that their response lies always in the linear elastic domain. The elastic properties of glass fiber and epoxy are reported in Table 1.

### 3. Vectorial formulation of the Virtual Crack Closure Technique (VCCT)

165 In order to express the VCCT formulation of the ERR in terms of FEM variables, we need to introduce a few rotation matrices in order to represent the discretized representation (FE mesh) of a crack along a circular interface. The position of the crack tip is characterized by the angular size of the crack (see Sec. 2 and Fig. 1 for reference) and the rotation corresponding to the crack tip  
170 reference frame is represented by the matrix  $\underline{\underline{R}}_{\Delta\theta}$  defined as

$$\underline{\underline{R}}_{\Delta\theta} = \begin{bmatrix} \cos(\Delta\theta) & \sin(\Delta\theta) \\ -\sin(\Delta\theta) & \cos(\Delta\theta) \end{bmatrix}. \quad (4)$$

Nodes belonging to the elements sharing the crack tip are involved in the VCCT estimation of the ERR and it is assumed that, given a sufficiently fine discretization, they are aligned with the crack propagation direction defined at the crack tip.

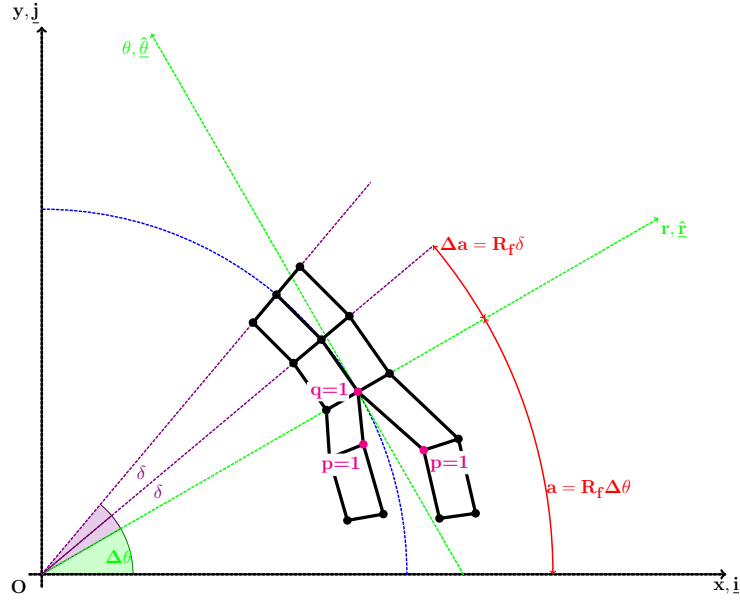
175 However, irrespectively of how small the elements in the crack tip neighborhood are, a misalignment always exists with respect to the assumed crack propagation direction (in the crack tip reference frame). This is measured by the matrices  $\underline{\underline{P}}_{\delta}(p)$ , defined as

$$\underline{\underline{P}}_{\delta}(p) = \begin{bmatrix} \cos\left(\left(1 + \frac{1-p}{m}\right)\delta\right) & \sin\left(\left(1 + \frac{1-p}{m}\right)\delta\right) \\ -\sin\left(\left(1 + \frac{1-p}{m}\right)\delta\right) & \cos\left(\left(1 + \frac{1-p}{m}\right)\delta\right) \end{bmatrix} \quad (5)$$

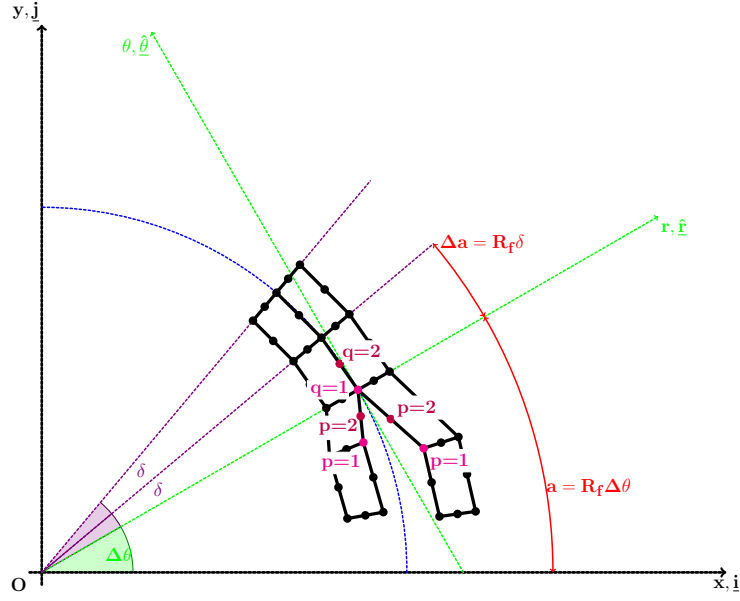
and  $\underline{\underline{Q}}_{\delta}(q)$ , equal to

$$\underline{\underline{Q}}_{\delta}(q) = \begin{bmatrix} \cos\left(\frac{q-1}{m}\delta\right) & \sin\left(\frac{q-1}{m}\delta\right) \\ -\sin\left(\frac{q-1}{m}\delta\right) & \cos\left(\frac{q-1}{m}\delta\right) \end{bmatrix}, \quad (6)$$





(a) Elements with 1<sup>st</sup> order shape functions:  $m = 1$  and  $p, q = 1$ .



(b) Elements with 2<sup>nd</sup> order shape functions:  $m = 2$  and  $p, q = 1, 2$ .

Figure 2: Schematic of the mesh at the fiber/matrix interface crack tip.

180 respectively for the free and bonded nodes involved in the VCCT estimation.  
 In Eqs. 5 and 6,  $\delta$  is the angular size of an element in the crack tip neighborhood  
 (see Sec. 2 and Fig. 1),  $m$  is the order of the element shape functions and  
 $p, q = 1, \dots, m$  are indices referring to the nodes belonging respectively to  
 free and bonded elements sharing the crack tip. Figure 2 shows the  $p, q$ -based  
 185 numbering of nodes at the crack tip in the case of elements with linear and  
 quadratic (serendipity) shape functions. Introducing the permutation matrix

$$\underline{\underline{P}}_\pi = \begin{bmatrix} 0 & 1 \\ -1 & 0 \end{bmatrix}, \quad (7)$$

it is possible to express the derivatives of rotation matrices  $\underline{\underline{R}}_{\Delta\theta}$ ,  $\underline{\underline{P}}_\delta$  and  $\underline{\underline{Q}}_\delta$   
 with respect to their argument:

$$\frac{\partial \underline{\underline{R}}_{\Delta\theta}}{\partial \Delta\theta} = \underline{\underline{P}}_\pi \cdot \underline{\underline{R}}_{\Delta\theta}, \quad \frac{\partial \underline{\underline{P}}_\delta}{\partial \delta} = \left(1 + \frac{1-p}{m}\right) \underline{\underline{P}}_\pi \cdot \underline{\underline{P}}_\delta, \quad \frac{\partial \underline{\underline{Q}}_\delta}{\partial \delta} = \frac{q-1}{m} \underline{\underline{P}}_\pi \cdot \underline{\underline{Q}}_\delta. \quad (8)$$

By means of Eqs. 5 and 6, we can express the crack tip forces  $\underline{\underline{F}}_{xy} = \begin{bmatrix} F_x \\ F_y \end{bmatrix}$   
 190 and crack displacements  $\underline{\underline{u}}_{xy} = \begin{bmatrix} u_x \\ u_y \end{bmatrix}$  in the crack tip reference frame (where the  
 tangential direction  $\theta$  correspond to the direction of crack propagation) while  
 taking into account the misalignment to the finite discretization as

$$\underline{\underline{F}}_{r\theta} = \underline{\underline{Q}}_\delta \underline{\underline{R}}_{\Delta\theta} \underline{\underline{F}}_{xy} \quad \underline{\underline{u}}_{r\theta} = \underline{\underline{P}}_\delta \underline{\underline{R}}_{\Delta\theta} \underline{\underline{u}}_{xy} \quad (9)$$

$$\text{where } \underline{\underline{F}}_{r\theta} = \begin{bmatrix} F_r \\ F_\theta \end{bmatrix} \text{ and } \underline{\underline{u}}_{r\theta} = \begin{bmatrix} u_r \\ u_\theta \end{bmatrix}.$$

The crack tip forces can be expressed as a function of the crack opening  
 195 displacement as

$$\underline{\underline{F}}_{xy} = \underline{\underline{K}}_{xy} \underline{\underline{u}}_{xy} + \tilde{\underline{\underline{F}}}_{xy}, \quad (10)$$

where  $\underline{\underline{K}}_{xy}$  is in general a full matrix of the form  $\underline{\underline{K}}_{xy} = \begin{bmatrix} K_{xx} & K_{xy} \\ K_{yx} & K_{yy} \end{bmatrix}$  and  $\tilde{\underline{F}}_{xy}$  represents the effect of the rest of the FE solution through the remaining nodes of the elements attached to the crack tip. As such, the term  $\tilde{\underline{F}}_{xy}$  can be expressed as a linear combination of the solution vector  $\underline{u}_N$  of nodal displacements of the form  $\tilde{\underline{\underline{K}}}_N \underline{u}_N$ . Equation 10 thus become

$$\underline{F}_{xy} = \underline{\underline{K}}_{xy} \underline{u}_{xy} + \tilde{\underline{\underline{K}}}_N \underline{u}_N. \quad (11)$$

An exemplifying derivation of the relationships expressed in Equations 10 and 11 can be found in Appendix A. It is worthwhile to observe that another author [37, 38] proposes a similar relationship, but in terms of flexibility  $\underline{u} = \underline{\underline{C}} \underline{F}$ . In [37, 38], Valvo expresses the forces at the crack tip as a (linear) function of the crack faces displacements at the same point. The technique analyzed in [37, 38] is the 2-steps VCCT [27]: given a structure with a crack of length  $a$ , a first simulation is run to compute the forces at the crack tip and, in the case, at the internal nodes of the first bonded element for  $p$ -refined meshes; then, a second simulation is conducted with the crack extended by  $\Delta a$ , where in practice  $\Delta a$  is the length of the element at the crack tip, and crack faces displacements are evaluated at the same nodes, now released, where previously forces were extracted. The Energy Release Rate is computed as the product of forces and displacements evaluated at the same nodes. The 2-steps VCCT adheres more strictly to the principle of the crack closure integral [13, 39]: the work needed to open the crack by  $\delta a$  (Energy Release Rate) is equal in magnitude to the work required to close it by the same amount. Forces and displacements should be thus evaluated at the same point respectively in the closed and open crack configuration. In this paper, we consider on the other hand the 1-step VCCT [27]: if the size of the elements at the crack tip is sufficiently small, the error committed by approximating the crack faces displacements at the crack tip with those one element before is negligible. This in turn eliminates the need for a second simulation and thus cut the required computational time by

a half. Following the principle of the crack closure integral [13, 39], Valvo's proposal is based on the observation that the crack face displacements at the crack tip for a virtual crack extension will be equal in magnitude and opposite in sign due the displacements caused by the application of crack tip forces. Thus, namely:  $u_{open\ crack} = -u_{closed\ crack} = f(F_{closed\ crack})$ , and for linear elastic materials  $f(F_{closed\ crack})$  would be linear, hence the introduction of a flexibility matrix [38]. Given that we instead work with the 1-step VCCT, we start from the observation that, in a Finite Element solution, the forces at a point can be expressed as a linear combination of all the displacements of the model through the global stiffness matrix. We have followed a stiffness approach and we have proceeded to isolate the contribution of crack faces displacements on crack tip forces. This leaves an additional term  $\tilde{\underline{K}}_N \underline{u}_N$  in Equation 11, which represents the contribution of the rest of the model and that is not present in Valvo's proposal. Notice that the linearity of Equation 11 does not stem from material linearity, but from the structure of the FEM solution. It can thus, in principle, be applied to non-linear materials, although as part of a secant- or tangent-based linearization. Notice that both the stiffness matrix of Equation 11 and Valvo's flexibility matrix possess out-of-diagonal elements, which represent the contribution of Poisson's effect. It is worthwhile to observe that another author [37] proposed a relationship of the form  $\underline{F}_{xy} = \underline{K}_{xy} \underline{u}_{xy}$ . However, in [37], this relationship is assumed *a priori* and manipulated to propose a revised version of the VCCT, based on the assumption that the matrix  $\underline{K}_{xy}$  should be diagonal to provide physically consistent fracture mode partitioning. On the other hand, in the present work we derive the relationships of Eqs. 10 and 11 from the formulation of the Finite Element Method. According to our derivation, it seems correct that the matrix  $\underline{K}_{xy}$  should not in general be diagonal in order to take into account Poisson's effect. In fact, a positive crack opening displacement would cause a transverse displacement in the neighborhood of the crack tip. Given that material properties are different on the two sides of a bi-material interface, a net shear would be applied to the crack tip which would correspond to a net contribution to the crack tip force related to crack shear displacement.

The analytical derivations presented in confirm these physical considerations.

255 Based upon the work of Raju [40], we introduce the matrix  $\underline{T}_{pq}$  to represent the weights needed in the VCCT to account for the use of singular elements. As already done previously, indices  $p$  and  $q$  refer to nodes placed respectively on the free (crack face) and bonded side of the crack tip. Nodes are enumerated so that the crack tip has always index 1, i.e. the higher the index the further  
 260 the node is from the crack tip. Matrix  $\underline{T}_{pq}$  has always a size of  $d \times d$ , where  $d = 2$  for a 2D problem and  $d = 3$  for a 3D problem. An element  $\underline{T}_{pq}(i, j)$  with  $i, j = 1, \dots, d$  represents the weight to be assigned to the product of component  $i$  of the displacement extracted at node  $p$  with component  $j$  of the force extracted at node  $q$ . The expression of  $\underline{T}_{pq}$  for quadrilateral elements with or  
 265 without singularity is reported in Appendix B. Notice that, given  $m$  is the order of the element shape functions, the element side has  $m + 1$  nodes and this represents the upper limit of indices  $p$  and  $q$ .

By using matrix  $\underline{T}_{pq}$ , it is possible to express the total ERR  $G$  evaluated with the VCCT as

$$G_{TOT} = \frac{1}{2R_f\delta} \sum_{p=1}^{m+1} \sum_{q=1}^{m+1} Tr \left( \underline{E}_{r\theta,q} \underline{u}_{r\theta,p}^T \underline{T}_{pq}^T \right), \quad (12)$$

270 where the symbol  $Tr$  stands for the *Trace* operator, which sums together the elements on the matrix main diagonal (first matrix invariant). Introducing the vector  $\underline{G} = \begin{bmatrix} G_I \\ G_{II} \end{bmatrix}$  of fracture mode ERRs, Mode I and Mode II ERR evaluated with the VCCT can be expressed as

$$\underline{G} = \frac{1}{2R_f\delta} \sum_{p=1}^{m+1} \sum_{q=1}^{m+1} Diag \left( \underline{E}_{r\theta,q} \underline{u}_{r\theta,p}^T \underline{T}_{pq}^T \right), \quad (13)$$

where  $Diag()$  is the function that extracts the main diagonal of the input  
 275 matrix as a column vector. Substituting Equations 9 and 11 in Equations 12 and 13, we can express the Mode I, Mode II and total Energy Release Rate as a function of the crack displacements and the FE solution (more details in

Appendix A) as

$$\begin{aligned}
G_{TOT} = & \frac{1}{2R_f\delta} \sum_{p=1}^{m+1} \sum_{q=1}^{m+1} Tr \left( \underline{Q}_{\underline{\delta}} \underline{R}_{\Delta\theta} \underline{K}_{xy,q} \underline{u}_{xy,q} \underline{u}_{xy,p}^T \underline{R}_{\Delta\theta}^T \underline{P}_{\underline{\delta}}^T \underline{T}_{pq}^T \right) + \\
& + \frac{1}{2R_f\delta} \sum_{p=1}^{m+1} \sum_{q=1}^{m+1} Tr \left( \underline{Q}_{\underline{\delta}} \underline{R}_{\Delta\theta} \tilde{\underline{F}}_{xy,q} \underline{u}_{xy,p}^T \underline{R}_{\Delta\theta}^T \underline{P}_{\underline{\delta}}^T \underline{T}_{pq}^T \right)
\end{aligned} \tag{14}$$

and

$$\begin{aligned}
\underline{G} = \begin{bmatrix} G_I \\ G_{II} \end{bmatrix} = & \frac{1}{2R_f\delta} \sum_{p=1}^{m+1} \sum_{q=1}^{m+1} Diag \left( \underline{Q}_{\underline{\delta}} \underline{R}_{\Delta\theta} \underline{K}_{xy,q} \underline{u}_{xy,q} \underline{u}_{xy,p}^T \underline{R}_{\Delta\theta}^T \underline{P}_{\underline{\delta}}^T \underline{T}_{pq}^T \right) + \\
& + \frac{1}{2R_f\delta} \sum_{p=1}^{m+1} \sum_{q=1}^{m+1} Diag \left( \underline{Q}_{\underline{\delta}} \underline{R}_{\Delta\theta} \tilde{\underline{K}}_{N,q} \underline{u}_N \underline{u}_{xy,p}^T \underline{R}_{\Delta\theta}^T \underline{P}_{\underline{\delta}}^T \underline{T}_{pq}^T \right)
\end{aligned} \tag{15}$$

#### 280 4. Rotational invariance of $G_{TOT}$

Recalling Equation 14 and observing that matrix  $\underline{T}_{pq}$  is always equal to the identity matrix pre-multiplied by a suitable real constant (see Eq. B.1 in Appendix B), the total Energy Release Rate can be rewritten as

$$\begin{aligned}
G_{TOT} = & \frac{1}{2R_f\delta} \sum_{p=1}^{m+1} \sum_{q=1}^{m+1} Tr \left( \underline{Q}_{\underline{\delta}} \underline{R}_{\Delta\theta} \left( \underline{K}_{xy,q} \underline{u}_{xy,q} + \tilde{\underline{F}}_{xy,q} \right) \underline{u}_{xy,p}^T \underline{T}_{pq}^T \underline{R}_{\Delta\theta}^T \underline{P}_{\underline{\delta}}^T \right) = \\
= & \frac{1}{2R_f\delta} \sum_{p=1}^{m+1} \sum_{q=1}^{m+1} Tr \left( \underline{Q}_{\underline{\delta}} \underline{R}_{\Delta\theta} \underline{F}_{xy,q} \underline{u}_{xy,p}^T \underline{T}_{pq}^T \underline{R}_{\Delta\theta}^T \underline{P}_{\underline{\delta}}^T \right),
\end{aligned} \tag{16}$$

where  $\underline{F}_{xy}$  and  $\underline{u}_{xy}$  are the vectors of respectively the crack tip forces and  
285 crack displacements in the global ( $x - y$ ) reference frame. Given that  $\underline{Q}_{\underline{\delta}}$ ,  $\underline{P}_{\underline{\delta}}$  and  $\underline{R}_{\Delta\theta}$  all represent a linear transformation (a rigid rotation in particular),

the invariance of the trace to linear transformations ensures that

$$\begin{aligned}
G_{TOT} &= \frac{1}{2R_f\delta} \sum_{p=1}^{m+1} \sum_{q=1}^{m+1} Tr \left( \underline{Q}_{\delta} \underline{R}_{\Delta\theta} \underline{F}_{xy,q} \underline{u}_{xy,p}^T \underline{T}_{pq}^T \underline{R}_{\Delta\theta}^T \underline{P}_{\delta}^T \right) = \\
&= \frac{1}{2R_f\delta} \sum_{p=1}^{m+1} \sum_{q=1}^{m+1} Tr \left( \underline{F}_{xy,q} \underline{u}_{xy,p}^T \underline{T}_{pq}^T \right).
\end{aligned} \tag{17}$$

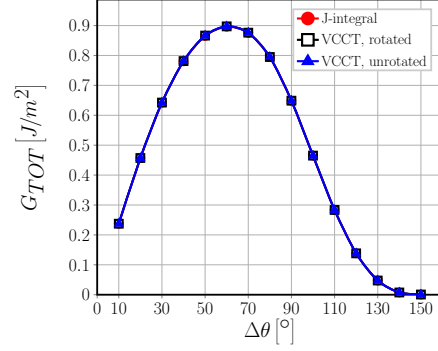
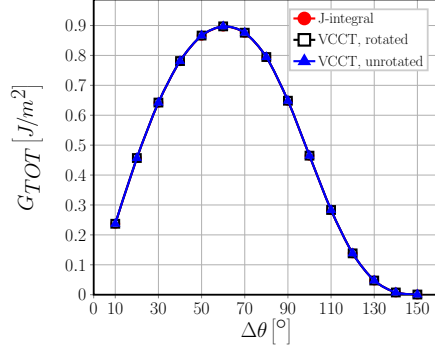
As  $G_{TOT}$  was defined according to Equation 12 and given that  $Tr(AB) = Tr(BA)$ , it holds that

$$\begin{aligned}
G_{TOT} &= \frac{1}{2R_f\delta} \sum_{p=1}^{m+1} \sum_{q=1}^{m+1} \underline{u}_{r\theta,p}^T \underline{T}_{pq}^T \underline{F}_{r\theta,q} = \frac{1}{2R_f\delta} \sum_{p=1}^{m+1} \sum_{q=1}^{m+1} Tr \left( \underline{F}_{r\theta,q} \underline{u}_{r\theta,p}^T \underline{T}_{pq}^T \right) = \\
&= \frac{1}{2R_f\delta} \sum_{p=1}^{m+1} \sum_{q=1}^{m+1} Tr \left( \underline{F}_{xy,q} \underline{u}_{xy,p}^T \underline{T}_{pq}^T \right) = \frac{1}{2R_f\delta} \sum_{p=1}^{m+1} \sum_{q=1}^{m+1} \underline{u}_{xy,p}^T \underline{T}_{pq}^T \underline{F}_{xy,q}
\end{aligned} \tag{18}$$

290 which shows that the total Energy Release Rate is invariant to rigid rotations  
and can be calculated equivalently with forces and displacements expressed in  
the local crack tip reference frame or the global reference frame. The analytical  
result is confirmed by the numerical solution of the fiber-matrix interface crack  
with different element orders and model fiber volume fractions, as shown in  
295 Figure 3.

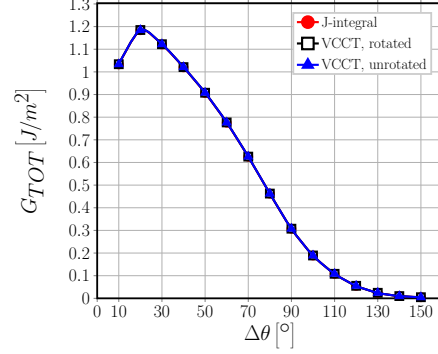
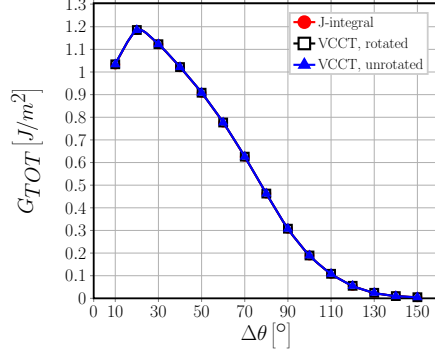
The result of Equation 18 has also physical implications:

- given that stress and displacement fields at the crack tip are the same, two  
cracks with different crack paths are energetically equivalent with respect  
to the total Energy Release Rate;
- 300 – given that laws of the type  $G_{TOT} \geq G_c$  govern crack propagation, if  $G_c$   
do not depend on mode ratio, crack orientation will not affect its growth.



(a)  $V_f = 0.1\%$ ,  $1^{st}$  order elements,  $\delta = 0.05^\circ$ .

(b)  $V_f = 0.1\%$ ,  $2^{nd}$  order elements,  $\delta = 0.05^\circ$ .



(c)  $V_f = 40\%$ ,  $1^{st}$  order elements,  $\delta = 0.05^\circ$ .

(d)  $V_f = 40\%$ ,  $2^{nd}$  order elements,  $\delta = 0.05^\circ$ .

Figure 3: Numerical invariance of the total Energy Release Rate:  $G_{TOT}$  computed with the VCCT with rotated forces and displacements (label *rotated*), with the VCCT with forces and displacements in the global reference frame (label *unrotated*) and with J-integral method (label *J-integral*).

## 5. Convergence analysis

### 5.1. Analytical considerations

Substituting Equations 8 in the derivative of Equation 13, we can investigate  
 305 the dependency of Mode I and Mode II ERR with respect to the size  $\delta$  of an



element in the crack tip neighborhood through

$$\begin{aligned}
\frac{\partial G}{\partial \delta} = & -\frac{1}{2R_f\delta^2} \sum_{p=1}^{m+1} \sum_{q=1}^{m+1} \text{Diag} \left( \underline{Q} \underline{R}_{\Delta\theta} \underline{K}_{xy} \underline{u}_{xy} \underline{u}_{xy}^T \underline{R}_{\Delta\theta}^T \underline{P}^T \underline{T}^T \right) - \frac{1}{2R_f\delta^2} \sum_{p=1}^{m+1} \sum_{q=1}^{m+1} \text{Diag} \left( \underline{Q} \underline{R}_{\Delta\theta} \underline{\tilde{K}}_N \underline{u}_N \underline{u}_{xy}^T \underline{R}_{\Delta\theta}^T \underline{P}^T \underline{T}^T \right) + \\
& + \frac{1}{2R_f\delta} \sum_{p=1}^{m+1} \sum_{q=1}^{m+1} \text{Diag} \left( \underline{Q} \underline{R}_{\Delta\theta} \underline{K}_{xy} \underline{u}_{xy} \underline{u}_{xy}^T \underline{R}_{\Delta\theta}^T \underline{P}^T \underline{D}^T \underline{T}^T \right) + \frac{1}{2R_f\delta} \sum_{p=1}^{m+1} \sum_{q=1}^{m+1} \text{Diag} \left( \underline{Q} \underline{R}_{\Delta\theta} \underline{\tilde{K}}_N \underline{u}_N \underline{u}_{xy}^T \underline{R}_{\Delta\theta}^T \underline{P}^T \underline{D}^T \underline{T}^T \right) + \\
& + \frac{1}{2R_f\delta} \sum_{p=1}^{m+1} \sum_{q=1}^{m+1} \text{Diag} \left( \underline{DQ} \underline{R}_{\Delta\theta} \underline{K}_{xy} \underline{u}_{xy} \underline{u}_{xy}^T \underline{R}_{\Delta\theta}^T \underline{P}^T \underline{T}^T \right) + \frac{1}{2R_f\delta} \sum_{p=1}^{m+1} \sum_{q=1}^{m+1} \text{Diag} \left( \underline{DQ} \underline{R}_{\Delta\theta} \underline{\tilde{K}}_N \underline{u}_N \underline{u}_{xy}^T \underline{R}_{\Delta\theta}^T \underline{P}^T \underline{T}^T \right) + \\
& + \frac{1}{2R_f\delta} \sum_{p=1}^{m+1} \sum_{q=1}^{m+1} \text{Diag} \left( \underline{Q} \underline{R}_{\Delta\theta} \underline{K}_{xy} \frac{\partial \underline{u}_{xy}}{\partial \delta} \underline{u}_{xy}^T \underline{R}_{\Delta\theta}^T \underline{P}^T \underline{T}^T \right) + \frac{1}{2R_f\delta} \sum_{p=1}^{m+1} \sum_{q=1}^{m+1} \text{Diag} \left( \underline{Q} \underline{R}_{\Delta\theta} \underline{\tilde{K}}_N \frac{\partial \underline{u}_N}{\partial \delta} \underline{u}_{xy}^T \underline{R}_{\Delta\theta}^T \underline{P}^T \underline{T}^T \right) + \\
& + \frac{1}{2R_f\delta} \sum_{p=1}^{m+1} \sum_{q=1}^{m+1} \text{Diag} \left( \underline{Q} \underline{R}_{\Delta\theta} \underline{K}_{xy} \underline{u}_{xy} \frac{\partial \underline{u}_{xy}^T}{\partial \delta} \underline{R}_{\Delta\theta}^T \underline{P}^T \underline{T}^T \right) + \frac{1}{2R_f\delta} \sum_{p=1}^{m+1} \sum_{q=1}^{m+1} \text{Diag} \left( \underline{Q} \underline{R}_{\Delta\theta} \underline{\tilde{K}}_N \underline{u}_N \frac{\partial \underline{u}_{xy}^T}{\partial \delta} \underline{R}_{\Delta\theta}^T \underline{P}^T \underline{T}^T \right); \tag{19}
\end{aligned}$$

which, after refactoring, provides

$$\begin{aligned}
\frac{\partial G}{\partial \delta} = & \frac{1}{\delta} G + \frac{1}{2R_f\delta} \sum_{p=1}^{m+1} \sum_{q=1}^{m+1} \text{Diag} \left( \underline{Q} \underline{R}_{\Delta\theta} \left( \underline{K}_{xy} \underline{u}_{xy} + \underline{\tilde{K}}_N \underline{u}_N \right) \underline{u}_{xy}^T \underline{R}_{\Delta\theta}^T \underline{P}^T \underline{D}^T \underline{T}^T \right) + \\
& + \frac{1}{2R_f\delta} \sum_{p=1}^{m+1} \sum_{q=1}^{m+1} \text{Diag} \left( \underline{DQ} \underline{R}_{\Delta\theta} \left( \underline{K}_{xy} \underline{u}_{xy} + \underline{\tilde{K}}_N \underline{u}_N \right) \underline{u}_{xy}^T \underline{R}_{\Delta\theta}^T \underline{P}^T \underline{T}^T \right) + \\
& + \frac{1}{R_f\delta} \sum_{p=1}^{m+1} \sum_{q=1}^{m+1} \text{Diag} \left( \underline{Q} \underline{R}_{\Delta\theta} \underline{K}_{xy} \frac{\partial \underline{u}_{xy}}{\partial \delta} \underline{u}_{xy}^T \underline{R}_{\Delta\theta}^T \underline{P}^T \underline{T}^T \right) + \frac{1}{2R_f\delta} \sum_{p=1}^{m+1} \sum_{q=1}^{m+1} \text{Diag} \left( \underline{Q} \underline{R}_{\Delta\theta} \underline{\tilde{K}}_N \frac{\partial \underline{u}_N}{\partial \delta} \underline{u}_{xy}^T \underline{R}_{\Delta\theta}^T \underline{P}^T \underline{T}^T \right) + \\
& + \frac{1}{2R_f\delta} \sum_{p=1}^{m+1} \sum_{q=1}^{m+1} \text{Diag} \left( \underline{Q} \underline{R}_{\Delta\theta} \underline{\tilde{K}}_N \underline{u}_N \frac{\partial \underline{u}_{xy}^T}{\partial \delta} \underline{R}_{\Delta\theta}^T \underline{P}^T \underline{T}^T \right). \tag{20}
\end{aligned}$$

Following the asymptotic analysis of [3, 1], in the case of an *open crack* the displacement in the crack tip neighborhood will have a functional form of the

310 type

$$u(\delta) \sim \sqrt{\delta} (\sin, \cos) (\epsilon \log \delta) \quad \text{with} \quad \epsilon = \frac{1}{2\pi} \log \left( \frac{1-\beta}{1+\beta} \right) \tag{21}$$

and  $\beta$  is Dundurs' parameter introduced in Section 1. Application of Equation 21 to the terms on the right hand side of Eq. 20 provides:

$$\underline{u}_{xy}, \underline{u}_N \sim u(\delta) \sim \sqrt{\delta} (\sin, \cos) (\epsilon \log \delta) \xrightarrow{\delta \rightarrow 0} 0; \tag{22}$$

$$\underline{u}_{xy} \underline{u}_{xy}^T, \underline{u}_N \underline{u}_N^T \sim u^2(\delta) \sim \delta (\sin^2, \cos^2, \sin \cdot \cos) (\epsilon \log \delta) \xrightarrow{\delta \rightarrow 0} 0; \tag{23}$$

$$\frac{\partial \underline{u}_{xy}}{\partial \delta} \underline{u}_{xy}^T, \frac{\partial \underline{u}_N}{\partial \delta} \underline{u}_{xy}^T \sim -\frac{1}{2} (\sin^2, \cos^2, \sin \cdot \cos) (\epsilon \log \delta) + (-\sin^2, \cos^2, \pm \sin \cdot \cos) (\epsilon \log \delta) \xrightarrow{\delta \rightarrow 0} \text{finite}; \quad (24)$$

$$\underline{G} \sim \frac{1}{\delta} \underline{u}_{xy} \underline{u}_{xy}^T \sim \frac{1}{\delta} u^2(\delta) \sim (\sin^2, \cos^2, \sin \cdot \cos) (\epsilon \log \delta) \xrightarrow{\delta \rightarrow 0} \text{finite}. \quad (25)$$

In Equations 22-25, the multiplication by a trigonometric function of the type  $(\sin, \cos, \sin^2, \cos^2, \sin \cdot \cos)$  prevents the divergence of the asymptote. Recalling  
 315 Eqs. 5 and 6, in the limit of  $\delta \rightarrow 0$  the rotation matrices become equal to the identity matrix:

$$\underline{P}_\delta, \underline{Q}_\delta \xrightarrow{\delta \rightarrow 0} \begin{bmatrix} 1 & 0 \\ 0 & 1 \end{bmatrix}. \quad (26)$$

Applying the results of Equations 22-26 to Eq. 20, it can be shown that the derivative of  $\underline{G}$  can be split in a factor that goes to 0 in the limit of  $\delta \rightarrow 0$  and in a factor independent of  $\delta$ :

$$\lim_{\delta \rightarrow 0} \frac{\partial \underline{G}}{\partial \delta} \sim \frac{1}{\delta} \left( \cancel{F(\delta)}^0 + \underline{C} \right). \quad (27)$$

320 Thus, asymptotically, the Mode I and Mode II Energy Release Rate behave like the logarithm of the angular size  $\delta$  of the elements in the crack tip neighborhood:

$$\lim_{\delta \rightarrow 0} \frac{\partial \underline{G}}{\partial \delta} \sim \frac{1}{\delta} \xrightarrow{\int d\delta} \lim_{\delta \rightarrow 0} \underline{G} \sim \underline{A} \log(\delta) + \underline{B}. \quad (28)$$

## 5.2. Numerical results

Evaluations of the Mode I, Mode II and total Energy Release Rate using  
 325 the VCCT applied to the FE solution of the fiber-matrix interface crack in the single fiber model of Sec. 2 are reported respectively in Fig. 4, Fig. 5 and Fig. 6.

Results for Mode I ERR in Fig. 4 show clearly the transition from the *open* crack regime, where Mode I ERR is different from zero, to the *closed* crack

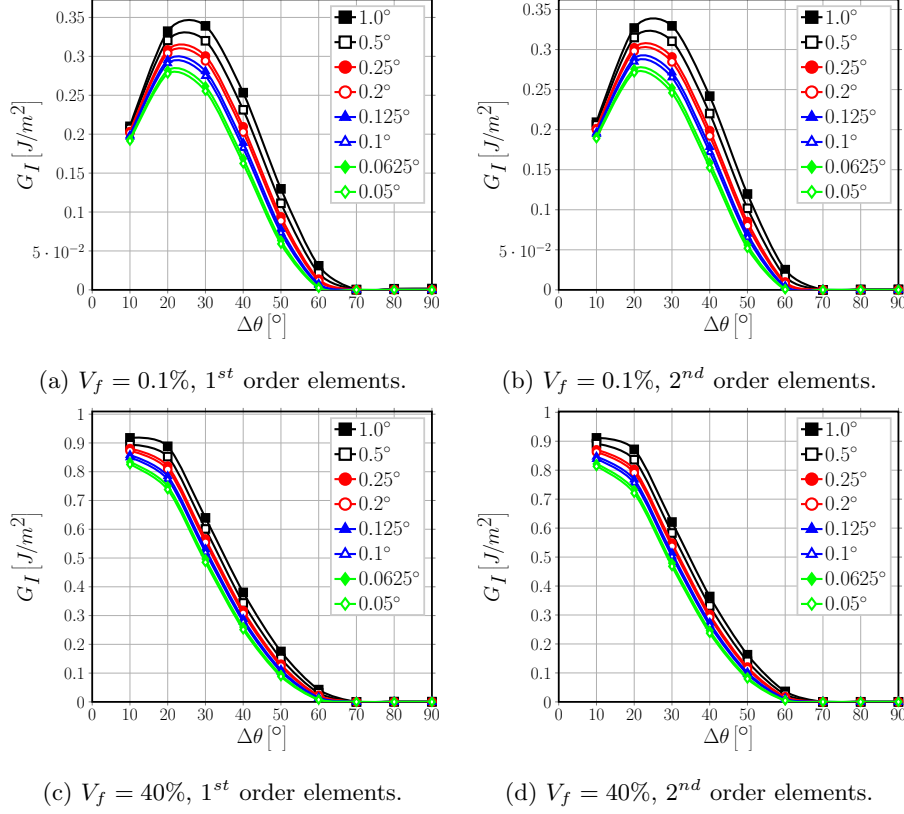


Figure 4: Effect of the size  $\delta$  of an element at the crack tip on Mode I ERR.

regime of the debond, where  $G_I = 0$ . Looking at Fig. 4, the crack is *open* for  
 330  $\Delta\theta \leq 60^\circ$  and it is *closed*, i.e. a contact zone is present, for  $\Delta\theta \geq 70^\circ$ . As  
 expected from the analysis of the previous section, and given that Mode I ERR  
 is different from zero only in the *open* crack regime, a significant dependence  
 on the element size  $\delta$  can be observed in Fig. 4 when using both  $1^{st}$  and  $2^{nd}$   
 order elements and with both an effectively infinite ( $V_f = 0.1\%$ ) and finite size  
 335 ( $V_f = 40\%$ ) matrix. At first sight, it is immediate to see from Fig. 4 that a  
 decrease in  $\delta$  leads to a decrease in  $G_I$ . However, two further effects can be  
 observed due to the refinement of the mesh at the crack tip, i.e. the decrease of  
 the element size  $\delta$ . First, the occurrence of the peak  $G_I$  is shifted to lower angles  
 for very low volume fractions: it occurs at  $\Delta\theta = 30^\circ$  with  $\delta = 1.0^\circ, 0.5^\circ$  and at

340  $\Delta\theta = 20^\circ$  with  $\delta \leq 0.25^\circ$  for both  $1^{st}$  and  $2^{nd}$  order elements and  $V_f = 0.1\%$ . Second, the appearance of the contact zone, i.e. the switch to the *closed* crack regime, is anticipated to smaller debonds: it occurs at  $\Delta\theta = 70^\circ$  with  $\delta \geq 0.2^\circ$  and at  $\Delta\theta = 60^\circ$  with  $\delta < 0.2^\circ$  for both  $1^{st}$  and  $2^{nd}$  order elements and both  $V_f = 0.1\%$  and  $V_f = 40\%$ .

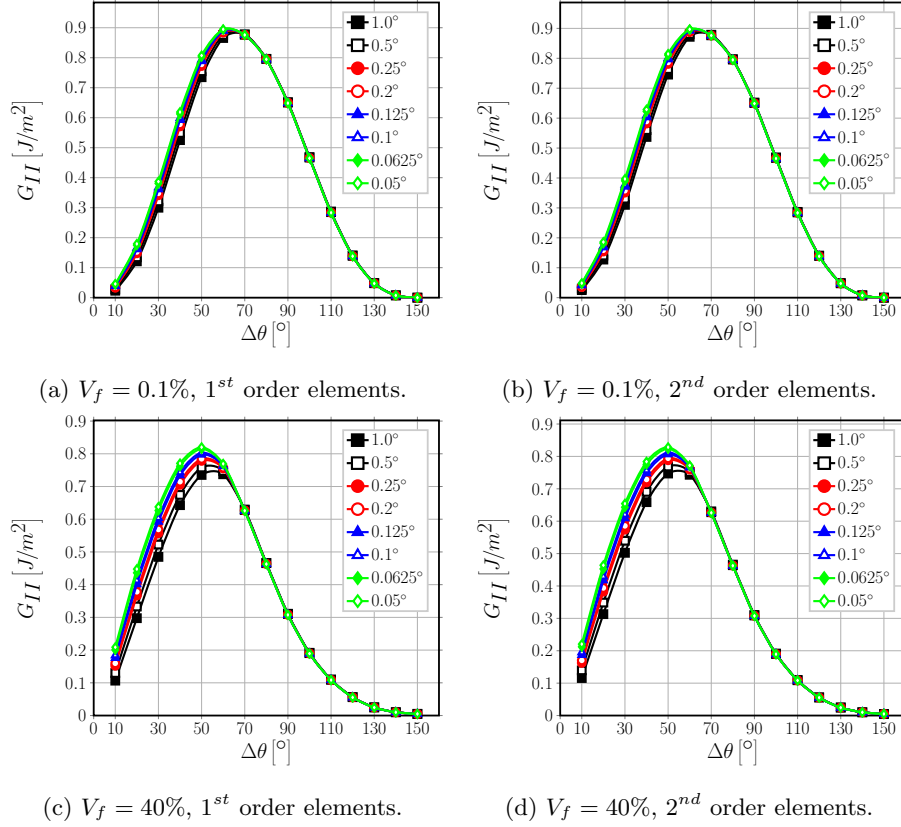


Figure 5: Effect of the size  $\delta$  of an element at the crack tip on Mode II ERR.

345 Observing Figure 5, it possible to notice the existence of two distinct regimes in the behavior of  $G_{II}$  with respect to the element size  $\delta$ . For  $\Delta\theta \leq 60^\circ$   $G_{II}$  depends on the value of  $\delta$ , while  $\Delta\theta \geq 70^\circ$  it is effectively independent of the element size at the crack tip for both  $1^{st}$  and  $2^{nd}$  order elements and both an effectively infinite ( $V_f = 0.1\%$ ) and finite size ( $V_f = 40\%$ ) matrix. Comparing  
350 the value of  $\Delta\theta$  at which the change from the  $\delta$ -dependency regime to the  $\delta$ -

independency regime occurs for  $G_{II}$  with Mode I ERR in Fig. 4, it is possible to observe that the  $\delta$ -dependency regime change of Mode II ERR coincides with the onset of the contact zone, i.e. the transition from *open* crack regime to the *closed* crack regime. The result confirms the analytical considerations of the previous section: for an *open* crack both Mode I and Mode II ERR depend on the element size  $\delta$  at the crack tip.

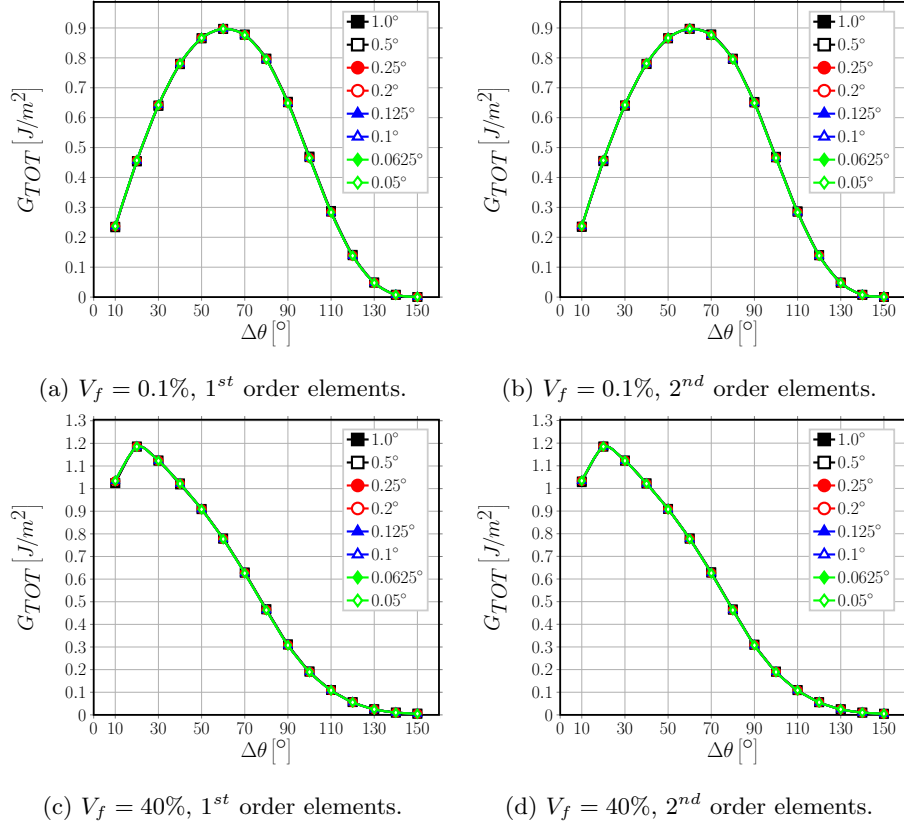


Figure 6: Effect of the size  $\delta$  of an element at the crack tip on total ERR.

Further observation of Figure 5 reveals that, in the *open* crack regime, decreasing the element size  $\delta$  causes an increase of Mode II ERR. Similarly to Mode I ERR, a shift of the peak  $G_{II}$  can also be observed for  $V_f = 0.1\%$ : the maximum value of  $G_{II}$  occurs at  $\Delta\theta = 70^\circ$  for  $\delta > 0.25^\circ$  for  $1^{st}$  order elements and for  $\delta > 0.5^\circ$  for  $2^{nd}$  order elements, while it is shifted to  $\Delta\theta = 60^\circ$  for

$\delta \leq 0.25^\circ$  for  $1^{st}$  order elements and for  $\delta \leq 0.5^\circ$  for  $2^{nd}$  order elements.

Table 2: Summary of linear regression results and main statistical tests for Mode I ERR

$V_f$ [%]	Order	$\Delta\theta$ [°]	$A$ [ $\frac{J}{m^2}$ ]	$B$ [ $\frac{J}{m^2}$ ]	$r$ [-]	$r^2$ [-]	$p(A)$ [-]	$p(B)$ [-]
0.1	1	10.0	0.0064	0.2113	0.9933	0.9866	7.48E-07	3.49E-14
		20.0	0.0183	0.3331	0.9996	0.9992	1.44E-10	2.40E-16
		30.0	0.0280	0.3392	1.0000	1.0000	2.25E-16	4.26E-21
		40.0	0.0304	0.2524	0.9997	0.9995	4.38E-11	7.94E-15
		50.0	0.0235	0.1278	0.9985	0.9970	8.61E-09	2.01E-11
		60.0	0.0094	0.0284	0.9854	0.9709	7.75E-06	6.14E-07
0.1	2	10.0	0.0069	0.2103	0.9962	0.9924	1.36E-07	1.03E-14
		20.0	0.0187	0.3277	0.9997	0.9994	7.85E-11	1.62E-16
		30.0	0.0280	0.3296	1.0000	1.0000	3.28E-16	7.29E-21
		40.0	0.0298	0.2408	0.9997	0.9995	4.82E-11	1.04E-14
		50.0	0.0225	0.1177	0.9984	0.9967	1.10E-08	3.27E-11
		60.0	0.0081	0.0228	0.9811	0.9626	1.66E-05	2.17E-06
40	1	10.0	0.0311	0.9196	0.9963	0.9927	1.03E-07	9.33E-15
		20.0	0.0501	0.8882	1.0000	0.9999	1.21E-13	2.33E-19
		30.0	0.0510	0.6374	0.9998	0.9996	1.66E-11	2.58E-16
		40.0	0.0419	0.3760	0.9988	0.9976	4.56E-09	5.25E-13
		50.0	0.0279	0.1713	0.9980	0.9961	2.22E-08	2.52E-11
		60.0	0.0108	0.0391	0.9901	0.9804	3.44E-06	9.46E-08
40	2	10.0	0.0336	0.9148	0.9988	0.9977	3.45E-09	5.09E-16
		20.0	0.0504	0.8719	1.0000	1.0000	3.70E-14	8.26E-20
		30.0	0.0506	0.6191	0.9999	0.9997	7.63E-12	1.35E-16
		40.0	0.0414	0.3608	0.9994	0.9989	4.95E-10	6.80E-14
		50.0	0.0269	0.1593	0.9982	0.9964	1.66E-08	2.31E-11
		60.0	0.0097	0.0329	0.9890	0.9781	4.96E-06	1.99E-07

Analysis of the total ERR in Figure 6 leads to an observation that was

not predicted by the considerations of the previous section:  $G_{TOT}$  is effectively  
 365 independent of the element size  $\delta$  in both the *open* and the *closed* crack regimes,  
 at least for reasonably small elements ( $\delta \leq 1.0^\circ$ ). Given that  $G_{II} = G_{TOT}$  for  
 the *closed* crack, it explains the independency of  $G_{II}$  from  $\delta$  after the onset of  
 the contact zone.

Analysis of Fig. 4, Fig. 5 and Fig. 6 has shown the dependency of Mode I and  
 370 Mode II ERR on the element size  $\delta$ . Following the derivations of the previous  
 section, we model the dependency of  $G_I$  and  $G_{II}$  with respect to  $\delta$  as

$$G_{(\cdot)} = A(\Delta\theta) \ln \delta + B(\Delta\theta), \quad (29)$$

where  $A(\Delta\theta)$  and  $B(\Delta\theta)$  are parameters dependent on  $\Delta\theta$  estimated through  
 linear regression (with  $x = \ln \delta$ ) of the numerical results.

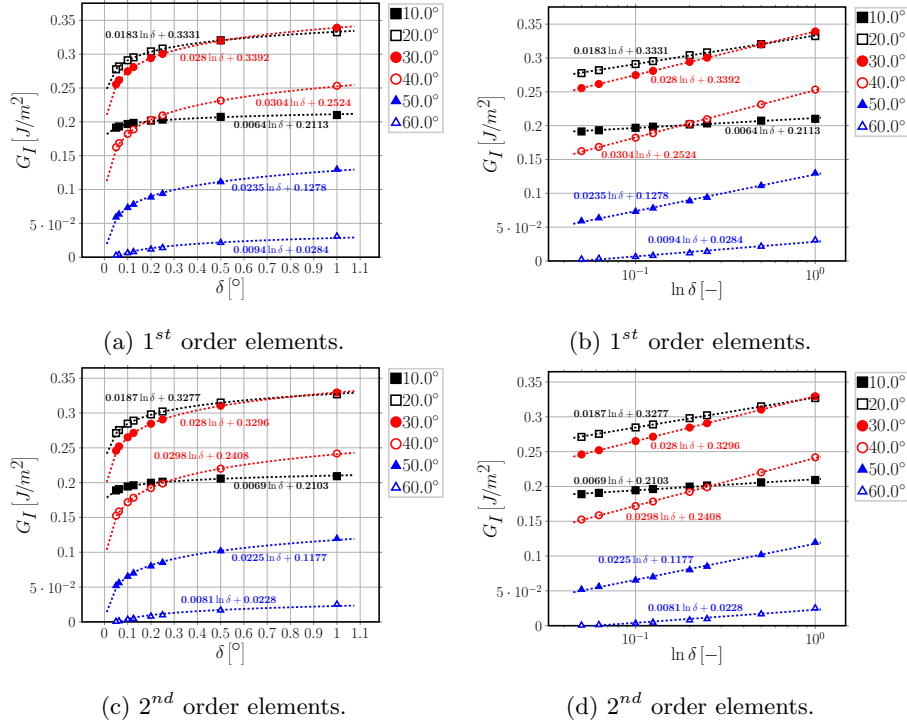


Figure 7: Logarithmic dependence on  $\delta$  of Mode I ERR: interpolation of numerical results for  $V_f = 0.1\%$ .

Table 3: Summary of linear regression results and main statistical tests for Mode II ERR

$V_f$ [%]	Order	$\Delta\theta$ [°]	$A$ [ $\frac{J}{m^2}$ ]	$B$ [ $\frac{J}{m^2}$ ]	$r$ [-]	$r^2$ [-]	$p(A)$ [-]	$p(B)$ [-]
0.1	1.0	10.0	-0.0076	0.0228	-0.9996	0.9991	2.09E-10	1.64E-11
		20.0	-0.0194	0.1211	-1.0000	1.0000	1.99E-15	2.02E-18
		30.0	-0.0290	0.3007	-0.9999	0.9998	4.12E-12	1.97E-16
		40.0	-0.0311	0.5270	-0.9995	0.9989	4.13E-10	1.05E-15
		50.0	-0.0240	0.7375	-0.9979	0.9958	2.32E-08	1.66E-15
		60.0	-0.0095	0.8685	-0.9835	0.9672	1.12E-05	1.22E-15
0.1	2.0	10.0	-0.0078	0.0249	-0.9996	0.9992	1.91E-10	1.06E-11
		20.0	-0.0196	0.1272	-1.0000	1.0000	3.48E-15	2.78E-18
		30.0	-0.0288	0.3108	-0.9999	0.9998	1.45E-12	5.47E-17
		40.0	-0.0305	0.5387	-0.9995	0.9990	3.32E-10	6.55E-16
		50.0	-0.0229	0.7478	-0.9979	0.9959	2.17E-08	1.09E-15
		60.0	-0.0082	0.8744	-0.9806	0.9615	1.81E-05	8.26E-16
40.0	1.0	10.0	-0.0344	0.1055	-0.9997	0.9995	3.82E-11	2.73E-12
		20.0	-0.0500	0.2977	-1.0000	0.9999	4.22E-14	5.66E-17
		30.0	-0.0505	0.4866	-0.9999	0.9997	6.44E-12	4.82E-16
		40.0	-0.0420	0.6454	-0.9996	0.9991	2.12E-10	9.66E-16
		50.0	-0.0275	0.7386	-0.9985	0.9971	9.01E-09	1.44E-15
		60.0	-0.0099	0.7402	-0.9926	0.9853	1.41E-06	5.13E-16
40.0	2.0	10.0	-0.0353	0.1145	-0.9998	0.9995	2.92E-11	1.50E-12
		20.0	-0.0504	0.3130	-1.0000	0.9999	4.00E-14	4.17E-17
		30.0	-0.0502	0.5039	-0.9999	0.9998	2.87E-12	1.69E-16
		40.0	-0.0410	0.6615	-0.9996	0.9992	2.02E-10	6.89E-16
		50.0	-0.0263	0.7502	-0.9987	0.9973	6.87E-09	7.76E-16
		60.0	-0.0090	0.7458	-0.9921	0.9842	1.79E-06	3.37E-16

As shown in Fig. 7, Fig. 8, Fig. 9 and Fig. 10 both in linear and logarithmic  
375 scales of  $\delta$ , the result is remarkable: both the correlation coefficient  $r$  and the



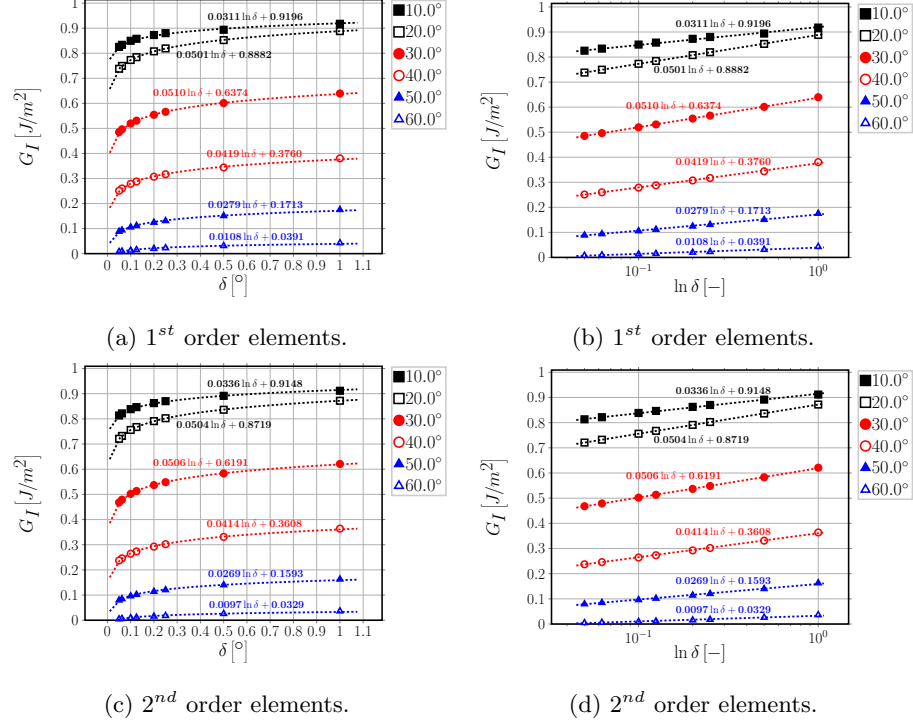


Figure 8: Logarithmic dependence on  $\delta$  of Mode I ERR: interpolation of numerical results for  $V_f = 40\%$ .

$r^2$  ratio (of explained to total variance) are always greater than 0.95 and the  $p$ -values of the coefficients  $A$  and  $B$  are at least  $< 1E - 6$  and often  $< 1E - 11$  (see Table 2 for  $G_I$  and Table 3 for  $G_{II}$ ). The results of the linear regression confirm the analytical derivations of the previous section, which showed the logarithmic behavior of Mode I and Mode II ERR. Similar conclusions were reached in [29, 31] for a straight bi-material crack with respect to the parameter  $\Delta a/a$ ; however, no functional expression of  $G_{(\cdot)}$  was proposed.

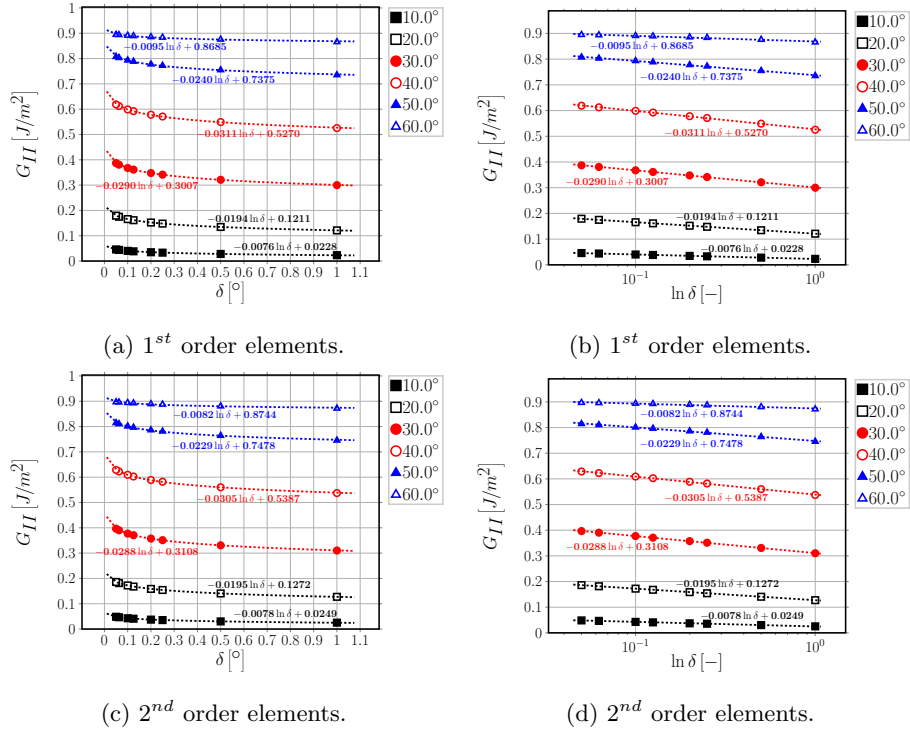


Figure 9: Logarithmic dependence on  $\delta$  of Mode II ERR: interpolation of numerical results for  $V_f = 0.1\%$ .

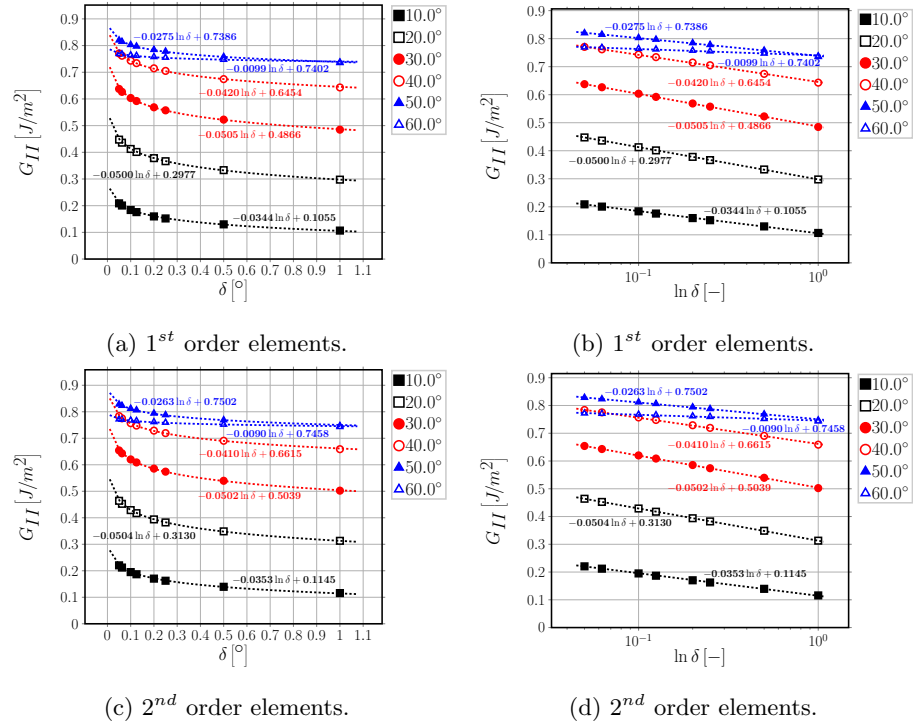


Figure 10: Logarithmic dependence on  $\delta$  of Mode II ERR: interpolation of numerical results for  $V_f = 40\%$ .

## 6. Conclusions & Outlook

The application of the Virtual Crack Closure Technique to the calculation of Mode I, Mode II and total Energy Release Rate was analyzed in the context of the Finite Element solution of the bi-material circular arc crack, or fiber-matrix interface crack. A synthetic vectorial formulation of the VCCT has been proposed and its usefulness exemplified in the analysis of the mesh dependency. By both analytical considerations and numerical simulations, it has been shown that:

- the total ERR is invariant to rotations of the reference frame (and more in general to linear transformations), which implies that rotation of crack tip forces and displacement is actually not required in the use of the VCCT for the calculation of  $G_{TOT}$ ;
- the total ERR does not depend on the size  $\delta$  of the elements at the crack tip, at least for reasonably small elements ( $\delta \leq 1.0^\circ$ ) ;
- as a consequence, Mode II ERR for the *closed* interface crack does not depend on  $\delta$ , as  $G_{II} = G_{TOT}$  after the onset of the contact zone;
- for the *open* interface crack, Mode I and Mode II ERR depend on the element size  $\delta$  through a logarithmic law of the type  $A(\Delta\theta) \ln \delta + B(\Delta\theta)$ ;
- the sign of the logarithm is always positive for  $G_I$ , i.e. it decreases when  $\delta$  decreases, and negative for  $G_{II}$ , i.e. it increases when  $\delta$  decreases.

The conclusion is significant: as the behavior of Mode I and Mode II is logarithmic with respect to mesh size, there exists no asymptotic limit and thus no convergence of the values. A convergence analysis based on the reduction of the error between successive iterations would not provide a reliable assessment of the accuracy of the FE solution of Mode I and Mode II Energy Release Rate of the fiber-matrix interface crack. A validation is thus required with respect to data obtained through a different method, be it analytical, numerical or experimental. Moreover, it has been shown that: first, the same behavior appears when

using  $1^{st}$  as well as  $2^{nd}$  order elements; second, no improvement is expected with the use of singular elements, as the logarithmic dependency of  $G_I$  and  $G_{II}$  is governed by the definition of ERR itself together with the asymptotic behavior of the displacement field at the crack tip. These two conclusions ~~put into discus-~~  
~~sion recommendations often provided by manuals of commercial FEM packages~~  
~~such as Abaqus [36]. The latter for example, in the context of VCCT-based crack~~  
~~propagation (Section 11.4.2 of the *Abaqus Analysis User's Guide*), suggests that~~  
~~in most cases mesh refinement will help with obtaining a realistic result, that~~  
~~results with nonlinear materials are more sensitive to meshing than results with~~  
~~small-strain linear elasticity and that first-order elements generally work best~~  
~~for crack propagation analysis. run contrary to the suggestions provided in the~~  
~~manuals of many commercial FEM packages, such as Abaqus [36] which suggests~~  
~~that (Section 11.4.2 of the *Abaqus Analysis User's Guide*): Sharp cracks (where~~  
~~the crack faces lie on top of one another in the undeformed configuration) are~~  
~~usually modeled using small-strain assumptions. Focused meshes, [...], should~~  
~~normally be used for small-strain fracture mechanics evaluations. However, for a~~  
~~sharp crack the strain field becomes singular at the crack tip. [...] In most cases~~  
~~the singularity at the crack tip should be considered in small-strain analysis~~  
~~(when geometric nonlinearities are ignored). Including the singularity often~~  
~~improves the accuracy of the J-integral, the stress intensity factors, and the~~  
~~stress and strain calculations because the stresses and strains in the region close~~  
~~to the crack tip are more accurate.. The previous considerations might apply for~~  
~~cracks in isotropic mediums; however, the VCCT-based crack propagation tech-~~  
~~nique is proposed in Abaqus as a suitable technique for surface-based simulation~~  
~~of bi-material interface debonding. We have shown that, for a circular interface~~  
~~crack: mesh-refinement ( $h$ -refinement) does not guarantee convergence of Mode~~  
~~I and Mode II ERR, as their dependency on element size is logarithmic; sensi-~~  
~~tivity to meshing is actually very significant in small-strain linear elasticity and~~  
~~depends on the nature of the linear elastic solution at the crack tip; no difference~~  
~~in convergence trends is observable between first and second order elements ( $p$ -~~  
~~refinement). This closing considerations are not meant to be a critique *per se* to~~

commercial software, but rather as a source for reflection on the best use of software tools. In this paper, we have shown how an established technique could still present issues worth to be investigated even when applied to a problem  
 445 with simple geometry and material behavior. Apart from the scientific merit of the results proposed, the conclusions presented here stand as an invitation to the practitioner to avoid black-box thinking and blind application of built-in software solutions. ~~We have shown that, in the context of the fiber/matrix interface crack, the convergence of the Energy Release Rate is determined by the~~  
 450 ~~asymptotic behavior of the elastic solution and only marginally by the choice of element order and type, thus contradicting the statements in [36].~~

## Acknowledgements

Luca Di Stasio thanks Prof. Janis Varna for the useful discussions and suggestions. Luca Di Stasio gratefully acknowledges the support of the European  
 455 School of Materials (EUSMAT) through the DocMASE Doctoral Programme and the European Commission through the Erasmus Mundus Programme.

## References

- [1] M. Comninou, An overview of interface cracks, *Engineering Fracture Mechanics* 37 (1) (1990) 197–208. doi:10.1016/0013-7944(90)90343-f.
- 460 [2] D. Hills, J. Barber, Interface cracks, *International Journal of Mechanical Sciences* 35 (1) (1993) 27–37. doi:10.1016/0020-7403(93)90062-y.
- [3] M. L. Williams, The stresses around a fault or crack in dissimilar media, *Bulletin of the Seismological Society of America* 49 (2) (1959) 199.
- 465 [4] J. Dundurs, Discussion: “edge-bonded dissimilar orthogonal elastic wedges under normal and shear loading” (bogy, d. b., 1968, *ASME j. appl. mech.*, 35, pp. 460–466), *Journal of Applied Mechanics* 36 (3) (1969) 650. doi:10.1115/1.3564739.

- [5] F. Erdogan, Stress distribution in a nonhomogeneous elastic plane with cracks, *Journal of Applied Mechanics* 30 (2) (1963) 232. doi:10.1115/1.3636517.
- [6] A. H. England, A crack between dissimilar media, *Journal of Applied Mechanics* 32 (2) (1965) 400. doi:10.1115/1.3625813.
- [7] B. Malyshev, R. Salganik, The strength of adhesive joints using the theory of cracks, *International Journal of Fracture Mechanics* 1-1 (2). doi:10.1007/bf00186749.  
URL <https://doi.org/10.1007/bf00186749>
- [8] M. Comninou, The interface crack, *Journal of Applied Mechanics* 44 (4) (1977) 631. doi:10.1115/1.3424148.  
URL <https://doi.org/10.1115/1.3424148>
- [9] A. H. England, An arc crack around a circular elastic inclusion, *Journal of Applied Mechanics* 33 (3) (1966) 637. doi:10.1115/1.3625132.
- [10] A. Perlman, G. Sih, Elastostatic problems of curvilinear cracks in bonded dissimilar materials, *International Journal of Engineering Science* 5 (11) (1967) 845–867. doi:10.1016/0020-7225(67)90009-2.
- [11] M. Toya, A crack along the interface of a circular inclusion embedded in an infinite solid, *Journal of the Mechanics and Physics of Solids* 22 (5) (1974) 325–348. doi:10.1016/0022-5096(74)90002-7.
- [12] F. París, J. C. Caño, J. Varna, The fiber-matrix interface crack — a numerical analysis using boundary elements, *International Journal of Fracture* 82 (1) (1996) 11–29. doi:10.1007/bf00017861.
- [13] G. R. Irwin, Fracture, in: *Elasticity and Plasticity / Elastizität und Plastizität*, Springer Berlin Heidelberg, 1958, pp. 551–590. doi:10.1007/978-3-642-45887-3\_5.

- [14] J. C. D. Caño, F. París, On stress singularities induced by the discretization in curved receding contact surfaces: a bem analysis, International Journal for Numerical Methods in Engineering 40 (12) (1997) 2301–2320. doi:10.1002/(sici)1097-0207(19970630)40:12<2301::aid-nme166>3.0.co;2-8.
- [15] J. Varna, F. París, J. C. Caño, The effect of crack-face contact on fiber/matrix debonding in transverse tensile loading, Composites Science and Technology 57 (5) (1997) 523–532. doi:10.1016/s0266-3538(96)00175-3.
- [16] F. París, E. Correa, V. Mantič, Kinking of transversal interface cracks between fiber and matrix, Journal of Applied Mechanics 74 (4) (2007) 703. doi:10.1115/1.2711220.
- [17] E. Correa, E. Gamstedt, F. París, V. Mantič, Effects of the presence of compression in transverse cyclic loading on fibre–matrix debonding in unidirectional composite plies, Composites Part A: Applied Science and Manufacturing 38 (11) (2007) 2260–2269. doi:10.1016/j.compositesa.2006.11.002.
- [18] E. Correa, V. Mantič, F. París, Effect of thermal residual stresses on matrix failure under transverse tension at micromechanical level: A numerical and experimental analysis, Composites Science and Technology 71 (5) (2011) 622–629. doi:10.1016/j.compscitech.2010.12.027.
- [19] E. Correa, F. París, V. Mantič, Effect of the presence of a secondary transverse load on the inter-fibre failure under tension, Engineering Fracture Mechanics 103 (2013) 174–189. doi:10.1016/j.engfracmech.2013.02.026.
- [20] E. Correa, F. París, V. Mantič, Effect of a secondary transverse load on the inter-fibre failure under compression, Composites Part B: Engineering 65 (2014) 57–68. doi:10.1016/j.compositesb.2014.01.005.



- [21] C. Sandino, E. Correa, F. París, Numerical analysis of the influence of a nearby fibre on the interface crack growth in composites under transverse tensile load, *Engineering Fracture Mechanics* 168 (2016) 58–75. doi:10.1016/j.engfracmech.2016.01.022.
- 525 [22] C. Sandino, E. Correa, F. París, Interface crack growth under transverse compression: nearby fibre effect, in: *Proceeding of the 18<sup>th</sup> European Conference on Composite Materials (ECCM-18)*, 2018.
- [23] L. Zhuang, A. Pupurs, J. Varna, R. Talreja, Z. Ayadi, Effects of inter-fiber spacing on fiber-matrix debond crack growth in unidirectional composites under transverse loading, *Composites Part A: Applied Science and Manufacturing* 109 (2018) 463–471. doi:10.1016/j.compositesa.2018.03.031.
- 530 [24] J. Varna, L. Q. Zhuang, A. Pupurs, Z. Ayadi, Growth and interaction of debonds in local clusters of fibers in unidirectional composites during transverse loading, *Key Engineering Materials* 754 (2017) 63–66. doi:10.4028/www.scientific.net/kem.754.63.
- 535 [25] L. Zhuang, R. Talreja, J. Varna, Transverse crack formation in unidirectional composites by linking of fibre/matrix debond cracks, *Composites Part A: Applied Science and Manufacturing* 107 (2018) 294–303. doi:10.1016/j.compositesa.2018.01.013.
- 540 [26] E. Rybicki, M. Kanninen, A finite element calculation of stress intensity factors by a modified crack closure integral, *Engineering Fracture Mechanics* 9 (4) (1977) 931–938. doi:10.1016/0013-7944(77)90013-3.
- [27] R. Krueger, Virtual crack closure technique: History, approach, and applications, *Applied Mechanics Reviews* 57 (2) (2004) 109. doi:10.1115/1.1595677.
- 545 [28] R. Krueger, K. N. Shivakumar, I. S. Raju, Fracture mechanics analyses for interface crack problems - a review, in: 54th

- 550 AIAA/ASME/ASCE/AHS/ASC Structures, Structural Dynamics, and  
Materials Conference, American Institute of Aeronautics and Astronautics,  
2013. doi:10.2514/6.2013-1476.
- [29] C. Sun, C. Jih, On strain energy release rates for interfacial cracks in bi-  
material media, *Engineering Fracture Mechanics* 28 (1) (1987) 13–20. doi:  
10.1016/0013-7944(87)90115-9.
- 555 [30] C. Sun, M. Manoharan, Strain energy release rates of an interfacial crack  
between two orthotropic solids, *Journal of Composite Materials* 23 (5)  
(1989) 460–478. doi:10.1177/002199838902300503.
- [31] M. Manoharan, C. Sun, Strain energy release rates of an interfacial crack  
between two anisotropic solids under uniform axial strain, *Composites Sci-*  
560 *ence and Technology* 39 (2) (1990) 99–116. doi:10.1016/0266-3538(90)  
90049-b.
- [32] I. Raju, J. Crews, M. Aminpour, Convergence of strain energy release  
rate components for edge-delaminated composite laminates, *Engineering*  
*Fracture Mechanics* 30 (3) (1988) 383–396. doi:10.1016/0013-7944(88)  
565 90196-8.
- [33] E. Glaessgen, W. Riddell, I. Raju, Effect of shear deformation and  
continuity on delamination modeling with plate elements, in: 39th  
AIAA/ASME/ASCE/AHS/ASC Structures, Structural Dynamics, and  
Materials Conference and Exhibit, American Institute of Aeronautics and  
570 Astronautics, 1998. doi:10.2514/6.1998-2023.
- [34] A. Agrawal, A. M. Karlsson, Obtaining mode mixity for a bimaterial inter-  
face crack using the virtual crack closure technique, *International Journal*  
*of Fracture* 141 (1-2) (2006) 75–98. doi:10.1007/s10704-006-0069-4.
- [35] S. Wang, C. Harvey, L. Guan, Partition of mixed modes in layered isotropic  
575 double cantilever beams with non-rigid cohesive interfaces, *Engineering*

Fracture Mechanics 111 (2013) 1–25. doi:10.1016/j.engfracmech.2013.09.005.

[36] Simulia, Providence, RI, USA, ABAQUS/Standard User’s Manual, Version 6.12 (2012).

580 [37] P. S. Valvo, A revised virtual crack closure technique for physically consistent fracture mode partitioning, International Journal of Fracture 173 (1) (2011) 1–20. doi:10.1007/s10704-011-9658-y.

[38] P. S. Valvo, A further step towards a physically consistent virtual crack closure technique, International Journal of Fracture 192 (2) (2015) 235–  
585 244. doi:10.1007/s10704-015-0007-4.

[39] G. R. Irwin, Analysis of stresses and strains near the end of a crack traversing a plate, Journal of Applied Mechanics - Transactions of the ASME E24 (1957) 351–369.

[40] I. Raju, Calculation of strain-energy release rates with higher order and  
590 singular finite elements, Engineering Fracture Mechanics 28 (3) (1987) 251–274. doi:10.1016/0013-7944(87)90220-7.

## **Appendix A. Derivation of the relationship between crack tip forces and displacements for first order quadrilateral elements**

### *Appendix A.1. Foundational relations*

595 We review and present in this Section the foundational relations of the isoparametric formulation of the Finite Element Method. The objective here is to provide a theoretical foundation to the expressions in Equation 10 and Equation 11 and a reference for the explicit calculation of the nodal stiffness matrices proposed in Eq. 10 and Eq. 11. We propose a general treatment, valid  
600 for 2- and 3-dimensional problems, so that the interested reader could evaluate the nodal stiffness matrices for both a 2- and a 3-dimensional crack. However, in order to clarify the structure of some specific objects, we explicitly write their

2-dimensional form, which is of interest for the problem of this paper.

Denoting by  $d$  the number of geometrical dimensions of the problem ( $d = 2$  in  
 605 the present work), the element Jacobian  $J$  and its inverse  $J^{-1}$  can be expressed  
 in general as

$$J_{ij} = (e_{\xi_j})_i = \frac{\partial x_i}{\partial \xi_j} \quad J_{ij}^{-1} = (e^{x_j})_i = \frac{\partial \xi_i}{\partial x_j} \quad i, j = 1, \dots, d \quad (\text{A.1})$$

where  $(e_{\xi_j})$  and  $(e^{x_j})$  are respectively the covariant and contravariant basis  
 vectors of the mapping between global  $\{x_i\}$  and local element  $\{\xi_i\}$  coordinates.  
 In 2D, assuming the global coordinates are  $\{x, y\}$  and the local element co-  
 610 ordinates are  $\{\xi, \eta\}$ , the covariant and contravariant basis vectors assume the  
 form

$$\underline{e}_\xi = \begin{bmatrix} \frac{\partial x}{\partial \xi} \\ \frac{\partial y}{\partial \xi} \end{bmatrix} \quad \underline{e}_\eta = \begin{bmatrix} \frac{\partial x}{\partial \eta} \\ \frac{\partial y}{\partial \eta} \end{bmatrix}, \quad (\text{A.2})$$

$$\underline{e}_x = \begin{bmatrix} \frac{\partial \xi}{\partial x} \\ \frac{\partial \eta}{\partial x} \end{bmatrix} \quad \underline{e}_y = \begin{bmatrix} \frac{\partial \xi}{\partial y} \\ \frac{\partial \eta}{\partial y} \end{bmatrix}. \quad (\text{A.3})$$

and the element Jacobian  $J$  and its inverse  $J^{-1}$  can be computed for a 2D  
 problem as

$$\underline{\underline{J}} = [\underline{e}_\xi | \underline{e}_\eta] = \begin{bmatrix} \frac{\partial x}{\partial \xi} & \frac{\partial x}{\partial \eta} \\ \frac{\partial y}{\partial \xi} & \frac{\partial y}{\partial \eta} \end{bmatrix} \quad \underline{\underline{J}}^{-1} = [\underline{e}^x | \underline{e}^y] = \begin{bmatrix} \frac{\partial \xi}{\partial x} & \frac{\partial \xi}{\partial y} \\ \frac{\partial \eta}{\partial x} & \frac{\partial \eta}{\partial y} \end{bmatrix}. \quad (\text{A.4})$$

where  $\{e_\xi, e_\eta\}$  and  $\{e^x, e^y\}$  are respectively the covariant and contravariant  
 615 basis vectors of the mapping between global  $\{x, y\}$  and local element  $\{\xi, \eta\}$   
 coordinates:

Denoting by  $d$  the number of geometrical dimensions of the problem ( $d = 2$   
 in the present work) and by  $\underline{p}$  the  $d \times 1$  position vector in global coordinates, we  
 can formally introduce the  $3(d-1) \times d$  matrix operator of partial differentiation  
 620  $\underline{\underline{\tilde{B}}}$  such that

$$\underline{\varepsilon}(\underline{p}) = \underline{\underline{\tilde{B}}} \cdot \underline{u}(\underline{p}), \quad (\text{A.5})$$

where  $\underline{u}$  and  $\underline{\varepsilon}$  are respectively the  $d \times 1$  displacement vector and the  $3(d-1) \times 1$  strain vector in Voigt notation. Denoting by  $n$  the number of nodes of a generic element, it holds that  $n = s \times m$  where  $s$  represents the number of sides of the element (3 for a triangle, 4 for a rectangle, ...) and  $m$  the order of the shape functions (1 for linear shape functions, 2 for quadratic shape functions, ...).  ~~$(n = s \times m$  where  $s$  represents the number of sides of the element and  $m$  the order of the shape functions)~~, We can now ~~We can furthermore~~ introduce the  $d \times d \cdot n$  matrix  $\underline{\underline{N}}$  of shape functions such that

$$\underline{u} = \underline{\underline{N}} \cdot \underline{u}_N, \quad (\text{A.6})$$

where  $\underline{u}_N$  is the  $d \cdot n \times 1$  vector of element nodal variables. Having introduced  $\underline{\underline{\tilde{B}}}$  and  $\underline{\underline{N}}$  in Equations A.5 and A.6 respectively, it is possible to define the  $3(d-1) \times d \cdot n$  matrix  $\underline{\underline{B}}$  of derivatives (with respect to global coordinates) of shape functions as

$$\underline{\underline{B}} = \underline{\underline{\tilde{B}}} \cdot \underline{\underline{N}}. \quad (\text{A.7})$$

We introduce the linear elastic material behavior in the form of the  $3(d-1) \times 3(d-1)$  rigidity matrix  $\underline{\underline{D}}$  such that

$$\underline{\underline{\sigma}} = \underline{\underline{D}} \cdot \underline{\underline{\varepsilon}}, \quad (\text{A.8})$$

where  $\underline{\underline{\sigma}}$  the  $3(d-1) \times 1$  stress vector in Voigt notation. It is finally possible to define the  $n \times n$  element stiffness matrix  $\underline{\underline{k_e}}$  as

$$\underline{\underline{k_e}} = \int_{V_e(x_i)} (\underline{\underline{B}}^T \underline{\underline{D}} \cdot \underline{\underline{B}}) dV_e(x_i) = \int_{V_e(\xi_i)} (\underline{\underline{B}}^T \underline{\underline{D}} \cdot \underline{\underline{B}}) \sqrt{g} dV_e(\xi_i), \quad (\text{A.9})$$

where  $g = \det(\underline{\underline{J}}^T \underline{\underline{J}})$  and  $V_e$  is the element volume. Given that isoparametric elements are always defined between  $-1$  and  $1$  in each dimension, Equation A.9 can simplified to

$$\underline{\underline{k_e}} = \int_{-1}^1 \cdots \int_{-1}^1 (\underline{\underline{B}}^T \underline{\underline{D}} \cdot \underline{\underline{B}}) \sqrt{g} d\xi_i, \quad (\text{A.10})$$

640

which is amenable to numerical integration by means of a Gaussian quadrature of the form

$$\underline{\underline{k}}_e \approx \underbrace{\sum_{k=1}^N \cdots \sum_{h=1}^N}_{d \text{ times}} w_k \dots w_h \left( \underline{\underline{B}}^T (\xi_i(k, \dots, h)) \cdot \underline{\underline{D}} \cdot \underline{\underline{B}} (\xi_i(k, \dots, h)) \sqrt{g} \right), \quad (\text{A.11})$$

where  $\xi_i(k, \dots, h)$  ( $\xi_i, \dots, \eta_j$ ) are the coordinates of the  $N$  Gaussian quadrature points. The element stiffness matrix as evaluated in Eq. A.11 is in general a full symmetric matrix in the case of linear elasticity. For 2D rectangular elements with quadratic shape functions (8-nodes serendipity elements), the element stiffness matrix has the form ~~The element stiffness matrix as evaluated in Eq. A.11 is in general a full symmetric (in the case of linear elasticity) matrix of the form~~

$$k_e = \begin{bmatrix} k_{e|11} & k_{e|12} & k_{e|13} & k_{e|14} & k_{e|15} & k_{e|16} & k_{e|17} & k_{e|18} \\ k_{e|12} & k_{e|22} & k_{e|23} & k_{e|24} & k_{e|25} & k_{e|26} & k_{e|27} & k_{e|28} \\ k_{e|13} & k_{e|23} & k_{e|33} & k_{e|34} & k_{e|35} & k_{e|36} & k_{e|37} & k_{e|38} \\ k_{e|14} & k_{e|24} & k_{e|34} & k_{e|44} & k_{e|45} & k_{e|46} & k_{e|47} & k_{e|48} \\ k_{e|15} & k_{e|25} & k_{e|35} & k_{e|45} & k_{e|55} & k_{e|56} & k_{e|57} & k_{e|58} \\ k_{e|16} & k_{e|26} & k_{e|36} & k_{e|46} & k_{e|56} & k_{e|66} & k_{e|67} & k_{e|68} \\ k_{e|17} & k_{e|27} & k_{e|37} & k_{e|47} & k_{e|57} & k_{e|67} & k_{e|77} & k_{e|78} \\ k_{e|18} & k_{e|28} & k_{e|38} & k_{e|48} & k_{e|58} & k_{e|68} & k_{e|78} & k_{e|88} \end{bmatrix}. \quad (\text{A.12})$$

#### Appendix A.2. Calculation of displacements and reaction forces

650

With reference to Fig. A.11, we define:

$u_{x,M}$ ,  $u_{x,F}$  the  $x$ -displacement of the nodes belonging to the free side of the first element belonging to the crack, respectively on the matrix (bulk) and fiber (inclusion) side;

655

$u_{y,M}$ ,  $u_{y,F}$  the  $y$ -displacement of the nodes belonging to the free side of the first element belonging to the crack, respectively on the matrix (bulk) and fiber (inclusion) side;

$u_{r,M}$ ,  $u_{r,F}$  the  $r$ -displacement of the nodes belonging to the free side of the first element belonging to the crack, respectively on the matrix (bulk) and fiber (inclusion) side;

660  $u_{\theta,M}$ ,  $u_{\theta,F}$  the  $\theta$ -displacement of the nodes belonging to the free side of the first element belonging to the crack, respectively on the matrix (bulk) and fiber (inclusion) side;

$F_{x,CT}$ ,  $F_{y,CT}$  respectively the  $x$ - and  $y$ -component of the reaction force at the crack tip;

665  $F_{r,CT}$ ,  $F_{\theta,CT}$  respectively the  $r$ - and  $\theta$ -component of the reaction force at the crack tip.

The  $x - y$  reference frame is the global reference frame, while the  $r - \theta$  reference frame is such that the  $\theta$  direction coincides with the crack propagation direction at the crack tip and  $r$  the in-plane normal to the propagation direction.  
670 For an arc-crack as the present one, the  $r$ -direction coincides with the radial direction of the inclusion.

The crack opening displacement  $u_r$  and the crack shear displacement  $u_\theta$  at the crack tip can thus be written as

$$u_r = \cos(\Delta\theta) u_x + \sin(\Delta\theta) u_y \quad u_\theta = -\sin(\Delta\theta) u_x + \cos(\Delta\theta) u_y, \quad (\text{A.13})$$

where  $u_x$  and  $u_y$  are defined as

$$u_x = u_{x,M} - u_{x,F} \quad u_y = u_{y,M} - u_{y,F} \quad (\text{A.14})$$

675 and  $2\Delta\theta$  is total angular size of the debond. The corresponding forces at the crack tip are

$$F_r = \cos(\Delta\theta) F_{x,CT} + \sin(\Delta\theta) F_{y,CT} \quad F_\theta = -\sin(\Delta\theta) F_{x,CT} + \cos(\Delta\theta) F_{y,CT}. \quad (\text{A.15})$$

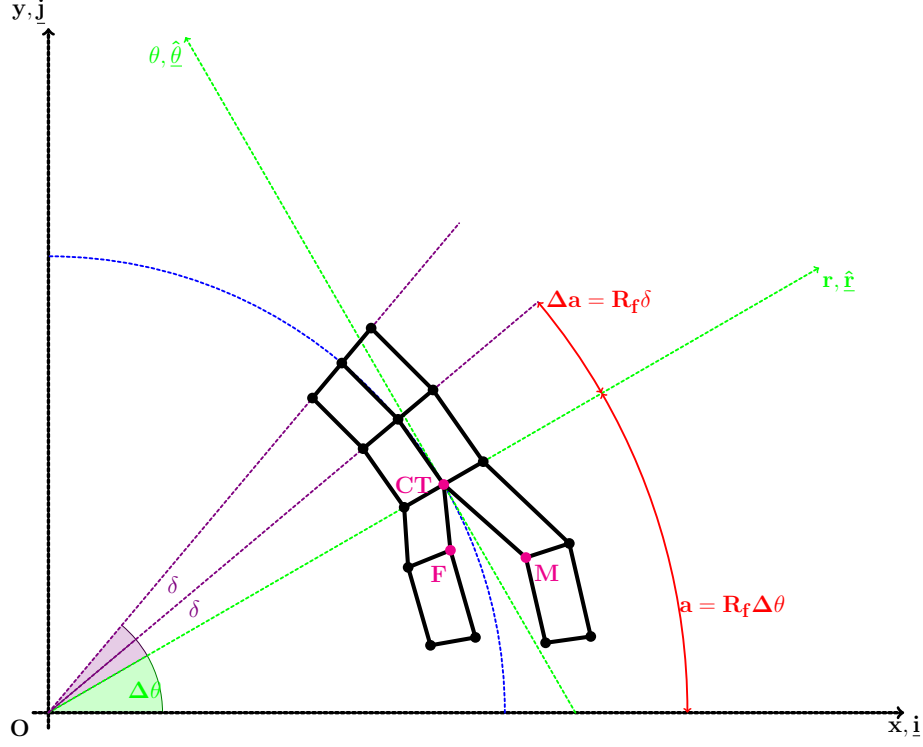


Figure A.11: Schematic representation of the discretized crack tip geometry for 1<sup>st</sup> order quadrilateral elements.

At the crack tip, the FE mesh possesses two coincident points, labeled  $FCT$  and  $MCT$ . Continuity of the displacements at the crack tip must be ensured. Furthermore, in order to measure the force at the crack tip, a fully-constraint dummy node needs to be created and formally linked to the two nodes at the crack tip by the conditions

$$\left\{ \begin{array}{l} u_{x,FCT} - u_{x,MCT} - u_{x,DUMMY} = 0 \\ u_{y,FCT} - u_{y,MCT} - u_{y,DUMMY} = 0 \\ u_{x,DUMMY} = 0 \\ u_{y,DUMMY} = 0 \end{array} \right. , \quad (A.16)$$



which can be simplified to

$$\left\{ \begin{array}{l} u_{x,FCT} = u_{x,MCT} \\ u_{y,FCT} = u_{y,MCT} \\ R_{x,DUMMY} = R_{x,FCT} = -R_{x,MCT} = F_{x,CT} \\ R_{y,DUMMY} = R_{y,FCT} = -R_{y,MCT} = F_{y,CT} \end{array} \right. . \quad (\text{A.17})$$

Making use of Eq. A.12, four equations can be written in the four displacement  $u_{x,FCT}$ ,  $u_{x,MCT}$ ,  $u_{y,FCT}$  and  $u_{y,MCT}$ :

$$\left\{ \begin{array}{l} (k_{e,M|11} + k_{e,M|33}) u_{x,MCT} + (k_{e,M|12} + k_{e,M|34}) u_{y,MCT} + \\ + k_{e,M|13} u_{x,M} + k_{e,M|14} u_{y,M} + (k_{M|17} + k_{M|35}) u_{N,MC|7} + (k_{M|18} + k_{M|36}) u_{N,MC|8} + \\ + \sum_{i=5}^6 k_{M|1i} u_{N,MC|i} + \sum_{i=7}^8 k_{M|3i} u_{N,MB|i} + k_{M|31} u_{x,NCOI} + k_{M|32} u_{y,NCOI} = 0 \\ \\ (k_{e,M|21} + k_{e,M|43}) u_{x,MCT} + (k_{e,M|22} + k_{e,M|44}) u_{y,MCT} + \\ + k_{e,M|23} u_{x,M} + k_{e,M|24} u_{y,M} + (k_{M|27} + k_{M|45}) u_{N,MC|7} + (k_{M|28} + k_{M|46}) u_{N,MC|8} + \\ + \sum_{i=5}^6 k_{M|2i} u_{N,MC|i} + \sum_{i=7}^8 k_{M|4i} u_{N,MB|i} + k_{M|41} u_{x,NCOI} + k_{M|42} u_{y,NCOI} = 0 \\ \\ (k_{e,F|77} + k_{e,F|55}) u_{x,FCT} + (k_{e,F|78} + k_{e,F|56}) u_{y,FCT} + \\ + k_{e,F|75} u_{x,F} + k_{e,F|76} u_{y,F} + (k_{F|71} + k_{F|53}) u_{N,FC|1} + (k_{F|72} + k_{F|54}) u_{N,FC|2} + \\ + \sum_{i=2}^3 k_{F|7i} u_{N,FC|i} + \sum_{i=1}^2 k_{F|5i} u_{N,FB|i} + k_{F|57} u_{x,NCOI} + k_{F|58} u_{y,NCOI} = 0 \\ \\ (k_{e,F|87} + k_{e,F|65}) u_{x,FCT} + (k_{e,F|88} + k_{e,F|66}) u_{y,FCT} + \\ + k_{e,F|85} u_{x,F} + k_{e,F|86} u_{y,F} + (k_{F|81} + k_{F|63}) u_{N,FC|1} + (k_{F|82} + k_{F|64}) u_{N,FC|2} + \\ + \sum_{i=2}^3 k_{F|8i} u_{N,FC|i} + \sum_{i=1}^2 k_{F|6i} u_{N,FB|i} + k_{F|67} u_{x,NCOI} + k_{F|68} u_{y,NCOI} = 0 \end{array} \right. . \quad (\text{A.18})$$

685

Solving for  $u_{y,FCT}$  and  $u_{y,MCT}$  the third and fourth relations in Eq. A.18

and substituting in the first two expressions of Eq. A.18, we get

$$\left\{ \begin{aligned}
 & (k_{e,M|11} + k_{e,M|33} + k_{e,F|77} + k_{e,F|55}) u_{x,MCT} + (k_{e,M|12} + k_{e,M|34} + k_{e,F|78} + k_{e,F|56}) u_{y,MCT} + \\
 & + k_{e,M|13} u_{x,M} + k_{e,M|14} u_{y,M} + k_{e,F|75} u_{x,F} + k_{e,F|76} u_{y,F} + \\
 & + (k_{M|31} + k_{F|57}) u_{x,NCOI} + (k_{M|32} + k_{F|58}) u_{y,NCOI} + \\
 & + (k_{M|17} + k_{M|35}) u_{N,MC|7} + (k_{M|18} + k_{M|36}) u_{N,MC|8} + (k_{F|71} + k_{F|53}) u_{N,FC|1} + (k_{F|72} + k_{F|54}) u_{N,FC|2} + \\
 & + \sum_{i=5}^6 k_{M|1i} u_{N,MC|i} + \sum_{i=7}^8 k_{M|3i} u_{N,MB|i} + \sum_{i=2}^3 k_{F|7i} u_{N,FC|i} + \sum_{i=1}^2 k_{F|5i} u_{N,FB|i} = 0 \\
 \\
 & (k_{e,M|21} + k_{e,M|43} + k_{e,F|87} + k_{e,F|65}) u_{x,MCT} + (k_{e,M|22} + k_{e,M|44} + k_{e,F|88} + k_{e,F|66}) u_{y,MCT} + \\
 & + k_{e,M|23} u_{x,M} + k_{e,M|24} u_{y,M} + k_{e,F|85} u_{x,F} + k_{e,F|86} u_{y,F} + \\
 & + (k_{M|41} + k_{F|67}) u_{x,NCOI} + (k_{M|42} + k_{F|68}) u_{y,NCOI} + \\
 & + (k_{M|27} + k_{M|45}) u_{N,MC|7} + (k_{M|28} + k_{M|46}) u_{N,MC|8} + (k_{F|81} + k_{F|63}) u_{N,FC|1} + (k_{F|82} + k_{F|64}) u_{N,FC|2} + \\
 & + \sum_{i=2}^3 k_{F|8i} u_{N,FC|i} + \sum_{i=1}^2 k_{F|6i} u_{N,FB|i} + \sum_{i=5}^6 k_{M|2i} u_{N,MC|i} + \sum_{i=7}^8 k_{M|4i} u_{N,MB|i} = 0
 \end{aligned} \right. \tag{A.19}$$

Solving the system of two equations and observing that  $u_{x,F}, u_{y,F} \sim 0$  for a stiffer inclusion as a fiber in a polymeric composite, we can express  $u_{x,MCT}$  as

a function of  $u_x$  and  $u_y$  (see Eq. A.14) as

$$\begin{aligned}
& \left[ (k_{e,M|21} + k_{e,M|43} + k_{e,F|87} + k_{e,F|65}) + \frac{k_{e,M|11} + k_{e,M|33} + k_{e,F|77} + k_{e,F|55}}{k_{e,M|12} + k_{e,M|34} + k_{e,F|78} + k_{e,F|56}} (k_{e,M|22} + k_{e,M|44} + k_{e,F|88} + k_{e,F|66}) \right] u_{x,MCT} + \\
& + \left( k_{e,M|23} - \frac{k_{e,M|22} + k_{e,M|44} + k_{e,F|88} + k_{e,F|66}}{k_{e,M|12} + k_{e,M|34} + k_{e,F|78} + k_{e,F|56}} k_{e,M|13} \right) u_x + \\
& + \left( k_{e,M|24} - \frac{k_{e,M|22} + k_{e,M|44} + k_{e,F|88} + k_{e,F|66}}{k_{e,M|12} + k_{e,M|34} + k_{e,F|78} + k_{e,F|56}} k_{e,M|14} \right) u_y + \\
& + \left( k_{e,M|23} + k_{e,F|85} - \frac{k_{e,M|22} + k_{e,M|44} + k_{e,F|88} + k_{e,F|66}}{k_{e,M|12} + k_{e,M|34} + k_{e,F|78} + k_{e,F|56}} (k_{e,M|13} + k_{e,M|75}) \right) \underline{u_{x,F}} \approx 0 + \\
& + \left( k_{e,M|24} + k_{e,F|86} - \frac{k_{e,M|22} + k_{e,M|44} + k_{e,F|88} + k_{e,F|66}}{k_{e,M|12} + k_{e,M|34} + k_{e,F|78} + k_{e,F|56}} (k_{e,M|14} + k_{e,M|76}) \right) \underline{u_{y,F}} \approx 0 + \\
& + \left[ (k_{M|41} + k_{F|67}) - \frac{k_{e,M|22} + k_{e,M|44} + k_{e,F|88} + k_{e,F|66}}{k_{e,M|12} + k_{e,M|34} + k_{e,F|78} + k_{e,F|56}} (k_{M|31} + k_{F|57}) \right] u_{x,NCOI} + \\
& + \left[ (k_{M|42} + k_{F|68}) - \frac{k_{e,M|22} + k_{e,M|44} + k_{e,F|88} + k_{e,F|66}}{k_{e,M|12} + k_{e,M|34} + k_{e,F|78} + k_{e,F|56}} (k_{M|32} + k_{F|58}) \right] u_{y,NCOI} + \\
& + (k_{M|27} + k_{M|45}) u_{N,MC|7} + (k_{M|28} + k_{M|46}) u_{N,MC|8} + (k_{F|81} + k_{F|63}) u_{N,FC|1} + (k_{F|82} + k_{F|64}) u_{N,FC|2} + \\
& - \frac{k_{e,M|22} + k_{e,M|44} + k_{e,F|88} + k_{e,F|66}}{k_{e,M|12} + k_{e,M|34} + k_{e,F|78} + k_{e,F|56}} [(k_{M|17} + k_{M|35}) u_{N,MC|7} + (k_{M|18} + k_{M|36}) u_{N,MC|8}] + \\
& - \frac{k_{e,M|22} + k_{e,M|44} + k_{e,F|88} + k_{e,F|66}}{k_{e,M|12} + k_{e,M|34} + k_{e,F|78} + k_{e,F|56}} [(k_{F|71} + k_{F|53}) u_{N,FC|1} + (k_{F|72} + k_{F|54}) u_{N,FC|2}] \\
& + \sum_{i=2}^3 k_{F|8i} u_{N,FC|i} + \sum_{i=1}^2 k_{F|6i} u_{N,FB|i} + \sum_{i=5}^6 k_{M|2i} u_{N,MC|i} + \sum_{i=7}^8 k_{M|4i} u_{N,MB|i} + \\
& - \frac{\sum_{i=5}^6 k_{M|1i} u_{N,MC|i} + \sum_{i=7}^8 k_{M|3i} u_{N,MB|i} + \sum_{i=2}^3 k_{F|7i} u_{N,FC|i} + \sum_{i=1}^2 k_{F|5i} u_{N,FB|i}}{k_{e,M|12} + k_{e,M|34} + k_{e,F|78} + k_{e,F|56}} = 0,
\end{aligned} \tag{A.20}$$

690

while the reaction forces at the crack tip can be expressed as

$$\left\{ \begin{array}{l} F_{x,CT} = R_{x,FCT} = \\ \quad = (k_{e,F|77} + k_{e,F|55}) u_{x,FCT} + (k_{e,F|78} + k_{e,F|56}) u_{y,FCT} + \\ \quad + k_{e,F|75} \underline{u_{x,F}} \approx 0 + k_{e,F|76} \underline{u_{y,F}} \approx 0 + \\ \quad + \sum_{i=1}^4 k_{e,F|7i} u_{N,FC|i} + \sum_{i=1, i \neq (5,6)}^8 k_{e,F|5i} u_{N,FB|i} \\ F_{y,CT} = R_{y,FCT} = \\ \quad = (k_{e,F|87} + k_{e,F|65}) u_{x,FCT} + (k_{e,F|88} + k_{e,F|66}) u_{y,FCT} + \\ \quad + k_{e,F|85} \underline{u_{x,F}} \approx 0 + k_{e,F|86} \underline{u_{y,F}} \approx 0 + \\ \quad + \sum_{i=1}^4 k_{e,F|8i} u_{N,FC|i} + \sum_{i=1, i \neq (5,6)}^8 k_{e,F|6i} u_{N,FB|i} \end{array} \right. . \tag{A.21}$$

Substituting Eq. A.18 in Eq. A.19, Eq. A.20 and Eq. A.21 and solving, we obtain an expression of the form

$$\left\{ \begin{array}{l} F_{x,CT} = K_{xx}u_x + K_{xy}u_y + \\ \quad + \sum_{i=1}^4 K_{FC,x|i}u_{N,FC|i} + \sum_{i=1,i \neq (3,4,5,6)}^8 K_{FB,x|i}u_{N,FB|i} + \\ \quad + \sum_{i=5}^8 K_{FC,x|i}u_{N,MC|i} + \sum_{i=7}^8 K_{MB,x|i}u_{N,FB|i} \\ F_{y,CT} = K_{yx}u_x + K_{yy}u_y + \\ \quad + \sum_{i=1}^4 K_{FC,y|i}u_{N,FC|i} + \sum_{i=1,i \neq (3,4,5,6)}^8 K_{FB,y|i}u_{N,FB|i} + \\ \quad + \sum_{i=5}^8 K_{FC,y|i}u_{N,MC|i} + \sum_{i=7}^8 K_{MB,y|i}u_{N,FB|i} \end{array} \right. , \quad (\text{A.22})$$

which can be reformulated synthetically as

$$\left\{ \begin{array}{l} F_{x,CT} = K_{xx}u_x + K_{xy}u_y + \tilde{F}_x \\ F_{y,CT} = K_{yx}u_x + K_{yy}u_y + \tilde{F}_y \end{array} \right. , \quad (\text{A.23})$$

where  $\tilde{F}_x$  and  $\tilde{F}_y$  represent the influence of the FE solution through the  
695 nodes of the elements sharing the crack tip that do not belong to any of the  
phase interfaces, i.e. the nodes of the elements sharing the crack tip that belong  
to the bulk of each phase.

## Appendix B. Expression of $\underline{T}_{pq}$ for quadrilateral elements with or without singularity

700 The expression of  $\underline{T}_{pq}$  for quadrilateral elements with or without singularity is

$$\begin{aligned}
 \underline{T}_{pq} &= \begin{cases} \underline{I} \text{ for } p = q < 2 \\ \underline{0} \text{ otherwise} \end{cases} && \text{for } 1^{st} \text{ order quadrilateral elements} \\
 &= \begin{cases} \underline{I} \text{ for } p = q < 3 \\ \underline{0} \text{ otherwise} \end{cases} && \text{for } 2^{nd} \text{ order quadrilateral elements} \\
 &= \begin{cases} \underline{I} \text{ for } p = q < 4 \\ \underline{0} \text{ otherwise} \end{cases} && \text{for } 3^{rd} \text{ order quadrilateral elements} \\
 &= \begin{cases} (14 - \frac{33\pi}{8}) \underline{I} \text{ for } p = 1, q = 1 \\ (-52 + \frac{33\pi}{2}) \underline{I} \text{ for } p = 1, q = 2 \\ (17 - \frac{21\pi}{4}) \underline{I} \text{ for } p = 2, q = 1 \\ (-\frac{7}{2} + \frac{21\pi}{16}) \underline{I} \text{ for } p = 2, q = 2 \\ (8 - \frac{21\pi}{8}) \underline{I} \text{ for } p = 1, q = 3 \\ (-32 + \frac{21\pi}{2}) \underline{I} \text{ for } p = 2, q = 3 \\ \underline{0} \text{ otherwise} \end{cases} && \text{for } 2^{nd} \text{ order quarter-point quadrilateral elements} \\
 &= \begin{cases} (-11187 + \frac{7155\pi}{2}) \underline{I} \text{ for } p = 1, q = 1 \\ (38556 - \frac{24543\pi}{2}) \underline{I} \text{ for } p = 1, q = 2 \\ (-53055 + \frac{33777\pi}{2}) \underline{I} \text{ for } p = 1, q = 3 \\ (\frac{11396}{3} - \frac{9575\pi}{8}) \underline{I} \text{ for } p = 2, q = 1 \\ (-12936 + \frac{33003\pi}{8}) \underline{I} \text{ for } p = 2, q = 2 \\ (17988 - \frac{45837\pi}{8}) \underline{I} \text{ for } p = 2, q = 3 \\ (-\frac{8453}{3} + \frac{3595\pi}{4}) \underline{I} \text{ for } p = 3, q = 1 \\ (9804 - \frac{12411\pi}{4}) \underline{I} \text{ for } p = 3, q = 2 \\ (-13587 + \frac{17289\pi}{4}) \underline{I} \text{ for } p = 3, q = 3 \\ (6948 - \frac{17685\pi}{8}) \underline{I} \text{ for } p = 1, q = 4 \\ (-23976 + \frac{60993\pi}{8}) \underline{I} \text{ for } p = 2, q = 4 \\ (33372 - \frac{84807\pi}{8}) \underline{I} \text{ for } p = 3, q = 4 \\ \underline{0} \text{ otherwise} \end{cases} && \text{for } 3^{rd} \text{ order quarter-point quadrilateral elements}
 \end{aligned}
 \tag{B.1}$$

where  $\underline{I}$  is the identity matrix.